



## **School of Chemistry**

Using nanostructured diamond surfaces to control bacterial adhesion and growth

James McGrath

**This thesis is submitted in partial fulfilment of the requirements for the Honours Degree of MSci (Bsc) at the University of Bristol**

Supervisor: Paul May

Second Assessor: Neil Fox

Physical and Theoretical Group

## Abstract

With growing concerns of bacterial resistance to antibiotics, novel methods of protecting surfaces from bacterial adhesion and proliferation are in high demand. This research focuses on a type of surfaces termed bactericidal; surfaces that kill bacterial upon adhesion. In particular, this work investigates materials that employ a physical mechanism of cell death, thus reducing antibiotic dependence. Black silicon (bSi) is one such surface, consisting of an array of silicon nano-needles which stretch and kill adhering cells. These needles are however very brittle, limiting the possible applications of bSi.

To improve the needle strength a diamond coating is grown over the needles, preserving the nanostructure of the surface. Both uncoated bSi and coated bSi (black diamond) have previously been proven to be bactericidal towards gram-negative bacteria, with the coating only slightly reducing the effectiveness.

This work investigates the bactericidal properties of diamond coated bSi against gram-positive bacteria, specifically *staphylococcus aureus*, and how the coating affects said properties. Fluorine termination was also performed on the surfaces to alter hydrophobicity; the effect on the bactericidal properties was also tested.

It was found the diamond coated black silicon produced was not bactericidal toward the gram-positive bacteria; death rates were as low as low as 17 %. Flat diamond controls tested displayed a higher percentage of cell death than black diamond. Fluorine termination slightly affected the properties, with a slightly higher rate of cell death than the H-terminated surface. Further, *S. Areus* demonstrated marginally higher adhesion toward the fluorine terminated surface.

## **Acknowledgements**

I would first like to thank my supervisor Paul May for all his help and guidance throughout the year, and for making my project so interesting. I would also like to thank Ed Smith for his endless help within the diamond lab, and the countless hours spent on the SEM getting our publication quality images. Lastly, thanks to Neil Fox for his insights along the way.

Special thanks are due to the research group at the University of Groningen which we worked with this year, for carrying out the biological testing involved in this project. Namely, Romana Schirhagl, Viraj Damale and Neda Norouzi.

# Contents

1	Introduction	6
1.1	Bacteria and Algae	6
1.1.1	Cell wall structure	7
1.1.2	Bacterial testing	8
1.2	Antibiofouling surfaces	9
1.3	Bactericidal Surfaces	10
1.3.1	Physical mechanism of cell death	13
1.4	Black silicon, bSi	14
1.5	Diamond	16
1.5.1	Surface termination	18
1.6	Previous work	20
1.7	Project aims	21
2	Methodology	22
2.1	Sample production	22
2.1.1	Black silicon, bSi	22
2.1.2	Seeding	22
2.1.3	Diamond growth	22
2.1.4	Termination	22
2.2	Characterisation	23
2.2.1	SEM	23
2.2.2	Water droplet contact angle	23
2.2.3	Raman	23
2.3	Bacterial testing	23
2.3.1	Culture production	23
2.3.2	Live/dead assay	23
2.3.3	CFU count assay	23
2.4	Black silicon production	24
3	Results and discussion	25
3.1	Black silicon	25
3.2	Black diamond	26
3.3	Water drop contact angle	30
3.4	Raman	32
3.5	Black silicon fabrication	34
3.6	Bactericidal results	38

	3.6.1	Cell death percentage .....	38
	3.6.2	Number of adhered cells .....	40
	3.6.3	CFU counts .....	42
4		Conclusion .....	44
5		Future work .....	45
6		Bibliography .....	46

# 1 Introduction

## 1.1 Bacteria and Algae

Bacterial infections and their subsequent complications are a constantly evolving problem faced within the medical sector. Current methods of preventing and controlling infections rely primarily upon antibiotics, an area which encounters a range of problems. New antibiotics are expensive to develop, with little chance of profitability; meaning fewer pharmaceutical companies are willing to invest time and money into their development.<sup>1</sup> With growing concerns of antibiotic resistant strains of bacteria, new methods of limiting such infections are being developed in an attempt to reduce the dependence we currently have on antibiotics.

The beginnings of a bacterial infection occur when bacteria adhere to a suitable, inert surface. At this stage, the bacteria are still susceptible to attack from antibiotics so the infection can be combated relatively easily. Given time the bacteria will begin to proliferate and irreversibly attach to the surfaces through the formation of a biofilm, an extracellular matrix of exopolysaccharides and proteins (Fig. 1), this process is termed biofouling.<sup>2</sup> Once a biofilm has been formed the bacteria within it are typically 10-500 times less sensitive to previously deadly antibiotics.<sup>3,4</sup> If a biofilm of pathogenic bacteria were to form within the body, for example upon an implant, the infection would be essentially untreatable by conventional methods.<sup>5</sup> The implant would have to be fully removed from the body, a very traumatic surgery for even the healthiest patients, and either replaced by a completely new implant or thoroughly cleaned and then put back into place.<sup>6</sup> With this in mind, development of surfaces that can prevent the formation of biofilms altogether (antibiofouling surfaces) is important for future protection against bacterial infection.

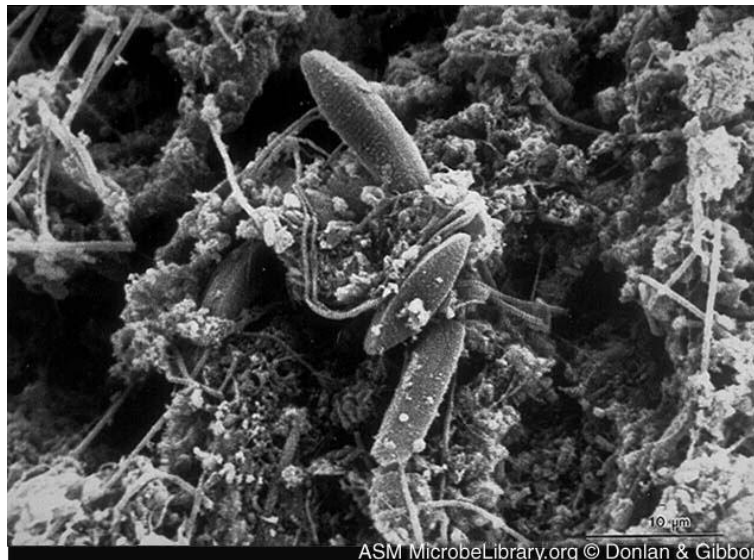


Figure 1. An SEM image of a biofilm formed upon a steel water pipe.

Although not related to bacteria, algae have some similar properties; most notably the ability to form biofilms on suitable surfaces.<sup>7</sup> Again, once fully formed the algae are very difficult to remove due to the multi-layered biofilm structure protecting the inner microorganisms.<sup>8</sup> Depending upon the surface on which they grow, the biofilms and any further algae growth can cause various problems; for example, decreasing the manoeuvrability of a boat and increasing fuel consumption by

up to 50%.<sup>9</sup> Many different methods of either removing or preventing algal biofilms have been developed, however no one current solution is suitable for all applications. For example, a Teflon non-stick coating requires flowing water to be effective, making them little use for the protection of jetties and other stationary objects. Current solutions include biocides such as copper oxides, which actively kill microorganisms attempting to attach<sup>10</sup>, and self-polishing paints which stop algae from binding in moving water.<sup>11</sup> In some applications a non-stick coating, typically fluorinated polymers, has proved to be a suitable method of protection from algal biofilms, this is also used to protect against bacterial biofilms.<sup>12</sup>

The process of bacterial adhesion depends upon many factors, most importantly the species of bacteria and the surface to which they adhere to. In this investigation the surface being adhered to is non-living or abiotic, this typically means adhesion proceeds via nonspecific interactions. The first phase of bacterial adhesion is the reversible docking phase, adhesion here is governed by a combination of forces, including but not limited to: van der Waals, steric interactions and electrostatic forces. The second stage is known as the locking or anchoring phase, this stage is typically irreversible. Bacteria that have begun to adhere produce and release exopolysaccharides, these complex with the surface, forming strong bonds to it.<sup>13</sup> During and after this stage other microorganisms are able to stick to any already bound cells with greater ease, increasing overall cell adhesion rates.<sup>14</sup>

### 1.1.1 Cell Wall Structure

Bacteria can be divided into two distinct classes: gram-positive and gram-negative (Fig. 2). This classification system was developed by Hans Gram in 1884 and is related to how different bacteria retain staining molecules.<sup>15</sup> The most important difference between them, in the scope of this work, is the structure of their cell walls. These two types of bacteria have a similar basic cell wall make-up, containing a phospholipid cell membrane, and a peptidoglycan layer which provides the walls rigidity.<sup>16</sup> The peptidoglycan layer of both is a biopolymer consisting of two amino sugars, N-acetylglucosamine (NAG) and N-acetylmuramic acid (NAM). The differences between the two classes of bacteria are the thickness and ordering of these two layers.

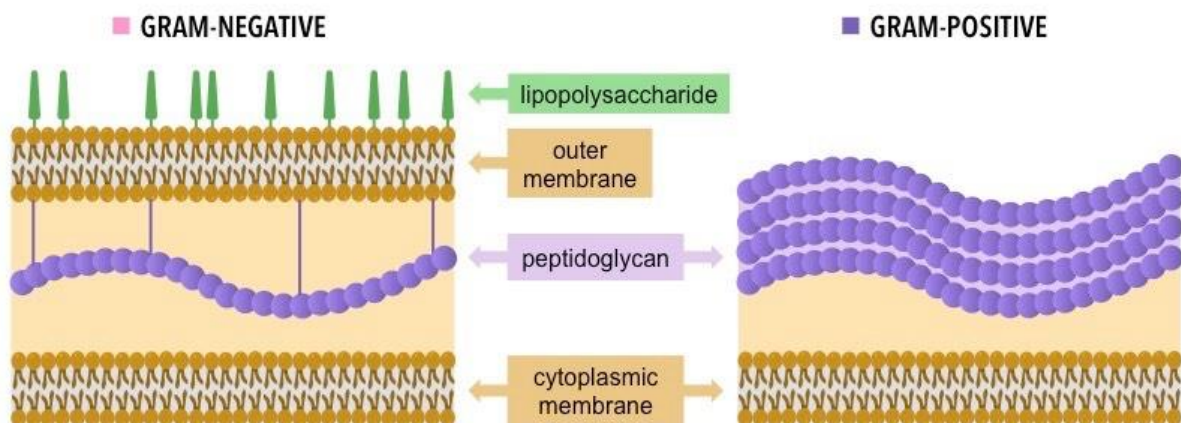


Figure 2. A basic depiction of the cell walls of gram-negative and gram-positive bacteria.

In gram negative bacteria the peptidoglycan layer is relatively thin, typically 7-8 nm, and is surrounded on either side by a phospholipid membrane. This additional membrane layer slows and prevents certain harmful compounds, such as penicillin, from entering the cell which affords gram-negative more resistance to antibiotics. The outermost layer is also responsible for the secretion of exopolysaccharides which allow the cell to adhere to surfaces.<sup>13</sup>

In comparison, Gram-positive bacteria have a much thicker peptidoglycan layer, roughly 4-5 times thicker; in some species this layer is up to 100 nm thick. The peptidoglycan layer accounts for 60-90 % of the cell wall, a far larger proportion than in gram-negative bacteria. Unlike gram-negative bacteria, the peptidoglycan layer is the outermost section of the cell wall, with no added protection this typically makes the cells more susceptible to antibiotic attack. However, the increased thickness of the peptidoglycan layer has other benefits, namely increased resistance to mechanical stress upon the cell, making cell rupture more difficult. The cell walls also retain their shape more effectively so will conform to a surface's topology to a lesser extent.

The strain of bacteria that will be used in this research is *staphylococcus aureus*, a gram-positive bacterium. Previous studies have been carried out into the structure of the cells wall of these bacteria, with findings relevant to this work. Analysis of the different compounds present within the cell wall found that the major component was N-acetylglucosamine, one of the two compounds which make up the peptidoglycan layer, suggesting this layer is thick in this bacterial species.<sup>17</sup> As previously noted, this thick layer will provide a large amount of rigidity in the cell wall, and likely make it resistant to external stresses. The diameter of these roughly spherical bacteria is shown, via SEM, to typically be less than a micron.

Algae are a very biodiverse group of organisms; some estimates predict the number of algae species to be over 1 million. This vast biodiversity results in a wide range of cell sizes, shapes and structures; within single cell species alone cell diameters range from 0.5 microns in *Prochlorococcus* to 1 mm in *Ethmodiscus*.<sup>18</sup> Similarly to both classes of bacteria, the cell wall of algae typically contains a layer of polysaccharide which provides the majority of the cell's structural integrity.<sup>19</sup> The thickness of this rigid layer is dependent upon the species of algae and can vary widely. It should be noted that some single celled green algae do not have a rigid cell wall, so this does not apply to these species.

### 1.1.2 Bacterial Testing

Bacteria upon a surface can be analysed in a number of ways, with each test providing different information. The first and one of the most widely used tests is a live/dead assay; this staining technique allows for differentiation between live and dead cells. In a typical live/dead assay, the dyes SYTO 9 and propidium iodide are used; SYTO 9 a cell-permeant dye that diffuses freely across membranes into live cells and into the nuclei, where it binds to nucleic acids and produces a green fluorescence. Upon binding to nucleic acids the dye is no longer membrane permeable, and so is retained by living cells. Although propidium iodide also intercalates nucleic acids, it is a very hydrophobic dye, and as such cannot cross cell membranes, instead it can only enter apoptotic cells with damaged membranes, where it produces a red fluorescence. Once bacteria upon a surface have been stained they are characterised via fluorescence microscopy to allow counting of live and dead cells.

Another test commonly employed is a colony forming unit (CFU) assay; a CFU assay estimates the number of cells or groups of cells, which have the ability to multiply under given conditions. For this test to be carried out the colonies have to be grown until visible to the eye, this is typically done by incubation at 37 °C for up to 24 hours after which colonies are counted. Using the dilution factor of

the applied bacterial solution, compared to the initial bacterial stock, and the volume of culture applied to the surface the results can be calculated.

## 1.2 Antibiofouling Surfaces

There are many known naturally occurring antibiofouling surfaces, many of which have this property due to their surface wettability; being either very hydrophobic or very hydrophilic, with each providing bacterial protection in different conditions.<sup>20</sup> Rather than killing bacteria, superhydrophobic surfaces reduce the bacteria's ability to adhere to the surface and therefore reduce the chance of biofilm formation.<sup>21</sup> One of the first examples of this found in nature was the Lotus leaf, with a very high water contact angle and a low slip angle (Fig. 3). When water comes into contact with the leaf it forms a ball and rolls off the leaf, as it moves it picks up any foreign bacteria leaving a cleaned surface behind.<sup>22</sup> Unfortunately this system of protection is only effective in applications where water will be present to clean the surface and remove foreign bodies.



Figure 3. A lotus leaf displaying superhydrophobic properties.

In an alternative manner, hydrophilicity can also protect a surface from bacterial adhesion in certain circumstances. This protection occurs through a layer of water being adsorbed onto the surface. The layer of water that forms on the surface reduces the ability of bacteria to adhere by inhibiting the initial docking phase of adhesion. It does this by introducing unfavourable hydrophobic interactions between the cell and the water layer.<sup>23</sup> The surface must therefore be in an aqueous environment all times or the surface will dry, limiting the possible applications of this method. In other cases, hydrophilic polymer can be added to a surface to reduce bacterial adhesion, these polymer chains themselves interfere with adhesion and can stop bacteria spreading over a surface.<sup>24</sup>

## 1.3 Bactericidal Surfaces

A material is said to be bactericidal if it kills bacterial cells upon contact, the mechanism of cell destruction can either be chemical or physical. Many of the naturally occurring bactericidal surfaces rely on physical methods of killing, rather than chemical methods which many man-made surfaces employ.<sup>25</sup> One such surface employing a chemical method, created by Aumsuwan et al, consists of a polymer layer to which penicillin is covalently attached; it was shown to be effective against *Staphylococcus aureus*, a gram-positive bacterium.<sup>26</sup> New methods of protection against bacterial infection are being developed to reduce our reliance on antibacterial chemicals.<sup>27</sup> This also aims to slow the prevalence of antibiotic resistant bacteria by making the use of antibiotics less common.

Other surfaces employ metal nanoparticles, which have been proven to have antibacterial properties. A range of different metals have been investigated and silver nanoparticles are widely regarded as the most effective antimicrobial agent; being able to kill bacteria, viruses and certain other micro-organisms.<sup>28</sup> Silver nanoparticles kill bacteria by distorting the cell wall, leading to cell death. The moisture exposed, outermost layer of silver is slowly oxidised which releases particles of ionised silver. These particles are highly reactive and bind to the structural proteins found within the bacteria cell wall, this process distorts and eventually kills the cell.<sup>29</sup> The nanoparticles are actively being depleted over time in this process, making this an unsuitable solution for many long-term applications.<sup>30</sup> One area they are still commonly used is in wound dressings as the nanoparticles have relatively low toxicity to humans and the required therapeutic window of the surface is low.<sup>31</sup>

A recent area of interest for bactericidal surfaces is surfaces that cause a physical method of cell death. This removes the concern of bacteria growing resistant to antibiotics and should also reduce constraints on the length of time that surfaces can be deployed whilst remaining effective. These surfaces typically have a specific nanostructure which makes them deadly to microorganisms that adhere to them. There are many naturally occurring bactericidal surfaces found throughout nature; this has prompted research into bio-inspired surfaces aiming to mimic the properties of said surfaces.<sup>25</sup>

Naturally occurring bactericidal surfaces typically rely upon some sort of surface protrusion on the nanoscale, for their bacterial resistance. The skin of a gecko is one such example, the skin is covered by an array of spinules or hairs, the hairs are typically a few microns long, have spacing of a few hundred nanometres and a slight curve (Fig. 4).<sup>32</sup> The skin is also superhydrophobic which provides some self-cleaning properties, similar to the lotus leaf. Watson *et al.* showed that gecko skin was bactericidal towards *Porphyromonas gingivalis*, a gram-negative strain of bacteria. The unique nanostructure of the gecko skin was synthetically replicated, through casting the skin, by Green *et al.*, the resulting surface was shown to be an effective bactericidal surface, with no decrease in efficacy compared to the skin itself.<sup>33</sup> This result suggests that the structure of the skin alone is responsible for its bactericidal properties.

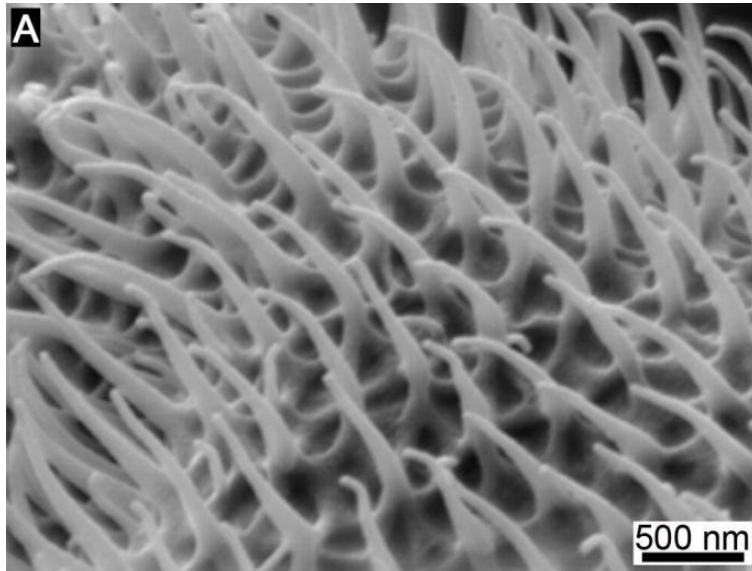


Figure 4. An SEM image of Gecko skin, showing the nano-structure responsible for its bactericidal properties.<sup>32</sup>

Whilst investigating the antibiofouling properties of the *Psaltoda claripennis* wings, a species of Cicada, Ivanova et al. discovered that the wings were actively killing bacteria that adhered to the surface.<sup>34</sup> It was previously thought that the wings relied upon their superhydrophobicity to provide a self-cleaning system of protection against bacteria. However, characterisation of the wings by electron microscopy revealed that the surface contained a hexagonal array of nanopillars; each pillar approximately 200 nm tall with an average spacing of 170 nm from centre to centre (Fig. 5). Biological testing was undertaken, and the wings were shown to be deadly towards *Pseudomonas aeruginosa*, a gram-negative bacterium. The wings killed most of the bacteria within 5 minutes of cell attachment.



Figure 5. A top down SEM image of the Cicada wing, showing the distribution of the nano-pillars.<sup>34</sup>

To prove that the structure of the wing is responsible for the bactericidal properties, the wings were coated in a thin layer, approximately 10 nm, of gold by magnetron sputtering, changing the hydrophobicity of the surface. The new surface was examined by atomic force microscopy and the topology was shown to be almost entirely unchanged. Biological testing was repeated upon the gold coated wings; the results showed no substantial change in the bactericidal activity of the wings. This

suggests that the nanostructure alone is responsible for the death of adhering bacteria, via a physical mechanism of cell rupture.

Further research was performed by Hasan et al., investigating the bactericidal properties of cicada wings toward different strains of bacteria, particularly gram-positive species.<sup>35</sup> The research looked at three gram-negative strains and three gram-positive strains and the wings were again shown to be effective against gram-negative strains, supporting the previous data (Fig. 6). However, the three strains of gram-positive bacteria were all shown to be resistant to cell rupture when adhering to the wings. As covered previously, the cell wall of gram-positive bacteria is multiple times thicker than those of gram-negative. It can be suggested that this increase in thickness will improve resistance to mechanical damage from the nanostructures.

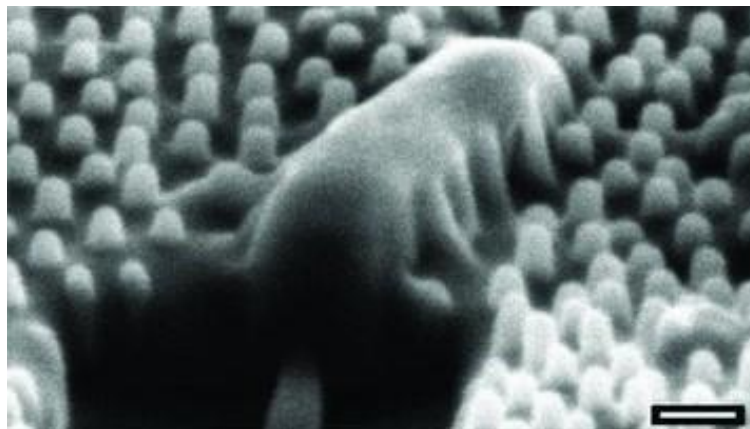


Figure 6. An SEM image of a *Pseudomonas aeruginosa* bacterium after adhering to a cicada wing.<sup>34</sup>

Research performed by Kelleher et al. investigated three different species of Cicada, comparing their nanostructures and the resulting bactericidal activity.<sup>36</sup> The authors found that the species with the tallest pillars and the tightest spacing, averaging 241 nm and 9 nm respectively, killed the highest percentage of bacteria that adhered. This suggests that the optimum surface properties for a bactericidal surface are taller pillars, packed tightly together. This work proposed that tighter spacing was effective as it resulted in more pillars making contact with each cell, something to be considered when investigating new surfaces.

In previous investigations, smaller gram-positive bacteria were seen to be resistant to the physical mechanisms of cell destruction employed by bactericidal surfaces.<sup>35</sup> However in 2012, Ivanova et al. discovered that the wings of the dragonfly *Diplacodes bipunctata*, were in fact bactericidal towards *S. aureus*.<sup>37</sup> This was the first reported case of a bactericidal surface killing gram-positive bacteria, this encouraged further research into the area as a broader range of bacteria could now be targeted. The nanostructure of the dragonfly wing appeared to be a lot more random than cicada wings; in both height of the pillars and their distribution. Typical heights were a few hundred nanometers, with average spacing of 90 nm.<sup>38</sup>

### 1.3.2 Physical mechanism of cell death

To explain the bactericidal nature of Cicada wings, Pogodin et al. developed a biophysical model of the interactions between the cell membrane of the bacteria and the surface of the wings.<sup>39</sup> It was suggested that adhesion of the cell onto the nanostructures of the wings greatly increases the total area of interaction between the two; resulting in the membrane stretching to cover the increased area. At a certain point, the membrane reaches its maximum stretching capability, so will rupture with any further adhesion down onto the nanostructures. This model relies on certain assumptions and simplifications; firstly, the cell wall is modelled as a thin elastic layer, ignoring the structural details. This can be done as the cell wall thickness (approximately 10 nm in gram-negative bacteria) is an order of magnitude smaller than the scale of the nanostructured surface (100s of nm). Again, due to differences in scale between pillar spacing and the cell itself, the curvature of the bacterial cell wall can also be ignored in the model.

The relatively simple model proposed is well summarised in the diagram below, the increasing area of adhesion ( $S_A$ ) and the portion of the cell that is under stress ( $S_B$ ) can be seen. At a certain point the stretching of the cell becomes too much and the cell wall will rupture. The diagram visualises how the cell wall is stretched as it tries to cover more and more of the surface.

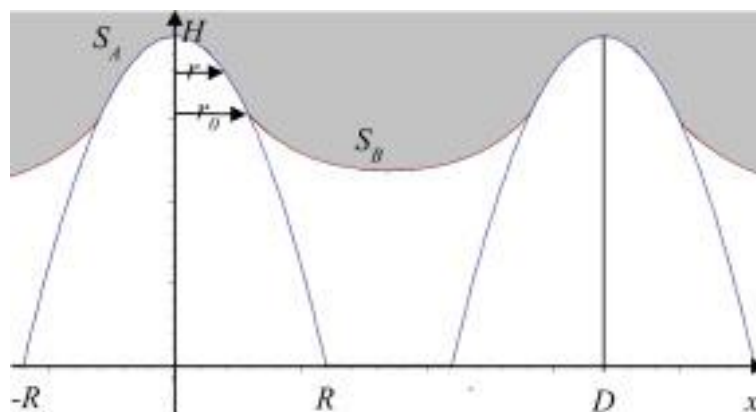


Figure 7. A side on, simplified depiction of a bacterial cell wall adhering to and stretching upon a nanostructured surface.<sup>40</sup>

Building upon this model, Xue et al. developed a more mathematically based model which aimed to explain in more detail how and why the structures of both the surface and the bacteria affected the cell rupture.<sup>40</sup> The model first defines the stretching degree as the difference in the area of the cell that is adhered to the surface ( $S_A$ ) and the area that is not ( $S_B$ ). When the degree of stretching reaches a certain maximum, the cell will rupture. The bacterial membrane is given a coefficient of stiffness, rather than being a thin elastic layer. The value of the stiffness depends upon the peptidoglycan layer; allowing the model to be applied more reliably to bacteria with different membrane thicknesses, i.e. gram-positive and gram-negative. By considering the strength of the covalent bonds that bridge peptidoglycan layers, numerical values can be calculated for the stiffness coefficient.

As it considers a wider range of variables, Xue's model can be used to determine the most efficient nanostructure that will result in cell rupture. For example, it was shown that the nano-pillars found on the surface of Cicada wings would be able to rupture the cell walls of gram-negative bacteria; but

most gram-positive bacteria would be resistant. This result aligns with the findings of Ivanova et al. in their investigations of the wing's bactericidal properties. Further investigation found that the thicker, gram-positive cell walls should rupture when the radius of the nano-pillar is reduced. This insight could prove helpful when developing bactericidal surfaces that can combat both types of bacteria.

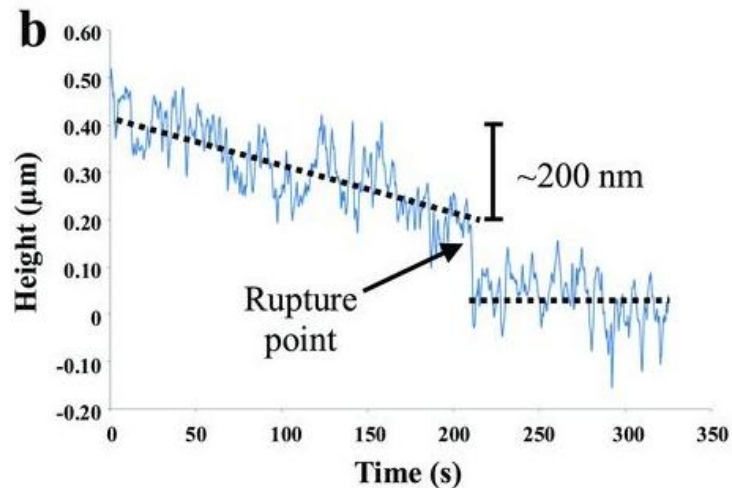


Figure 8. A graph displaying the height of a bacterial cell as it adheres to and sinks into a cicada wing.<sup>34</sup>

There is also some physical data which supports the mechanism proposed in the above work. It was carried out by Ivanova et. al. and used atomic force microscopy to measure the depth a bacterial cell sinks into a surface over time (Fig. 8). The cells slowly sink into the surface over time; for the surface and bacteria tested this proceeds until the cells are approximately 200 nm deep below the surface. After this point is reached, the cells rapidly drop until they are almost completely below the surface of sample (the needle tips). This suggests that at this depth below the surface the structure of the cells change, considering the mechanism covered above it is very likely that this is the rupturing of the cells. If the cells have ruptured and lost their rigidity it makes sense that they sink rapidly into the surface.

### 1.3 Black Silicon

Black silicon is a uniquely nanostructured material; made from a single silicon wafer that has been etched, typically by reactive ion etching (RIE).<sup>41</sup> Initially produced as an unwanted side product of etching in the 1980s, research into the material didn't begin until 1995.<sup>42</sup> The material consists of an array of silicon needles, the heights of the needles varies massively depending upon the etching conditions, typical heights range from 1 micron to several tens of microns (Fig. 9). The spacing of the needles can also be varied to alter the materials properties. The process of fabricating black silicon typically requires the use of the plasma of two different gases, the first of which etches away the silicon while the second plasma reacts with the new surface and passivates it, removing any residual reactivity.<sup>43</sup> The result is high aspect ratio needles of pure silicon that can be reproducibly manufactured. There are other methods that can be used to fabricate black silicon, but the etching

process is commonly used as it is more straightforward to fine tune the conditions and therefore the structure.

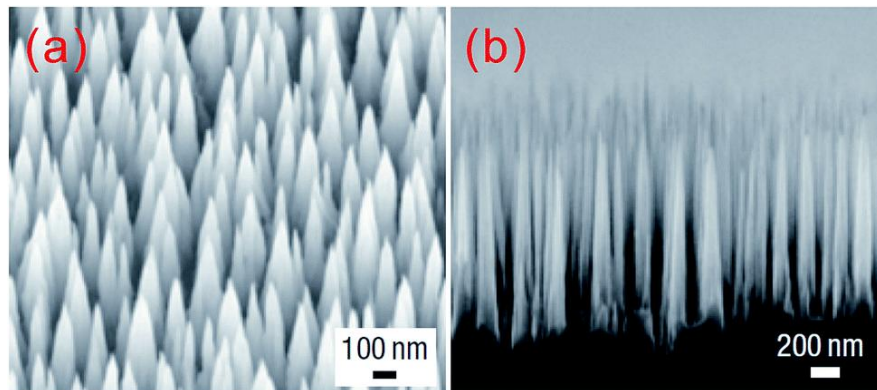


Figure 9. SEM images of (a) a tilted view of black silicon, (b) a side on view of the same sample.

The name black silicon arose due to the materials very low reflectivity and high absorbance of incoming light, together these properties result in a very deep black colour. The high absorbance can be attributed to the surface morphology; the pillars have a light trapping effect as they are on a similar scale to the wavelengths of the incoming light.<sup>44</sup> This property makes black silicon an attractive material for use in solar cells as almost 100% of light is being absorbed.<sup>45</sup> Black silicon can be doped to make it conductive; this doped material is being investigated for use in electrochemical cells due to the very high surface area to electrode area ratio.<sup>46</sup>

Following their studies on natural bactericidal surfaces, Ivanova et al. observed that black silicon had a similar nanostructure to the cicada wings. This prompted the first reported study into black silicon's bactericidal properties against both gram-positive and gram-negative bacteria.<sup>35</sup> Black silicon was found to be highly effective against *P. aeruginosa*, gram-negative, and *S. aureus*, gram-positive with cell killing rates against both bacteria of approximately  $450,000 \text{ cells min}^{-1} \text{ cm}^{-2}$ . A second gram-positive bacteria, *Bacillus subtilis*, was also tested; the rate of cell death was lower at  $150,000 \text{ cells min}^{-1} \text{ cm}^{-2}$ .

Although black silicon appears promising for bactericidal applications, the fragility of the material is of concern.<sup>47</sup> Previous work on bSi has reported that the high aspect ratio needles are prone to damage from minute forces.<sup>46</sup> This would drastically limit possible applications as once the needles are damaged the bactericidal properties are diminished. Loss of bactericidal properties is not the only issue that arises from structural damage; when snapped off the needles are very similar in size and shape to asbestos, posing a health risk to anyone exposed. These concerns led to a method of strengthening the needles being developed; growth of a diamond film over the needles. This technique retains the topology of the material, and therefore its bactericidal properties, whilst improving durability; allowing a larger range of real-world applications.

## 1.4 Diamond

Diamond is an allotrope of carbon with a highly regular, tetrahedral lattice of singly covalently bonded carbon atoms. This structure results in remarkable properties; diamond is the hardest known material, has the highest known thermal conductivity of any natural material and is chemically inert to all chemical reagents at room temperature. This combination of properties makes diamond suitable for many applications, from cutting tool coatings to optical lenses.<sup>48, 49</sup>

Diamond is naturally formed underground where pressure and temperature are extremely high, this combination of conditions results in naturally occurring carbon being converted to its diamond allotrope. Due to its high cost and relative scarcity research into diamond was limited at first, this was until 1955 when Bundy et. al. developed a high pressure, high temperature (HPHT) method of diamond synthesis.<sup>50</sup> Although this was a breakthrough, the method had drawbacks; the conditions required made it expensive and the diamonds grown were only single crystals. Research into diamond growth continued, and work by Eversole has shown that it was possible to grow diamonds layer by layer using gases at much lower pressure than HPHT methods.<sup>51</sup> This process, Hot Filament Chemical Vapour Deposition (HFCVD) used filaments heated to above 1000 °C. However, the growth of the resulting diamond was very slow and in addition layers of  $sp^2$  graphite were being deposited, resulting in low quality diamond films.

Building upon previous work, Angus et al developed a method of CVD diamond growth that incorporated hydrogen gas. The hydrogen etched away any graphite that was deposited resulting in a pure, polycrystalline diamond film.<sup>52</sup> The diamond films that this method produces lend themselves to a much wider range of applications than single crystal diamonds, CVD also has the advantage that the diamond can be grown directly onto a variety of substrates.<sup>53</sup>

CVD diamond growth proceeds through a series of chemical and physical processes. The first stage is the introduction of the reactant gases; typically a dilute mixture (c.a 1%) of methane in hydrogen, this will also include dopants if growing a doped diamond film. The gases diffuse through the reaction chamber towards the substrate but before reaching the substrate they encounter the high temperature filament, entering what is called the activation zone.<sup>54</sup> Here the high temperature and resulting transfer of energy causes the gas molecules to fragment forming highly reactive radicals.

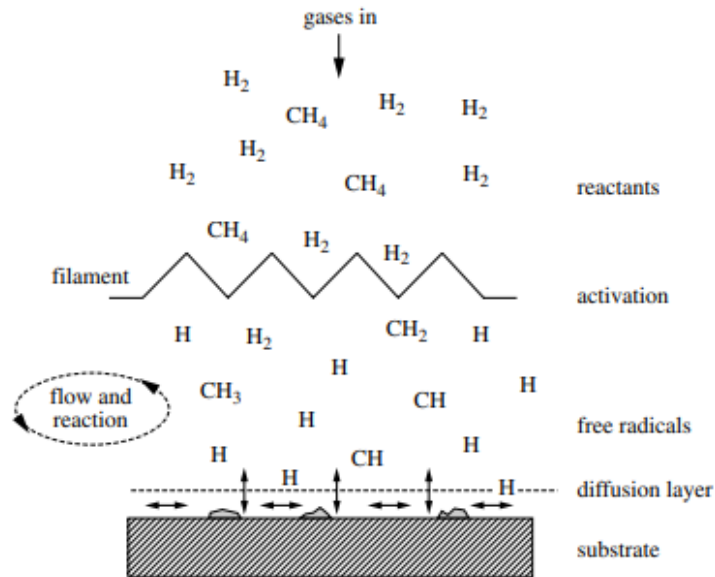


Figure 10. A schematic of the basic processes occurring inside a CVD reactor.<sup>55</sup>

The newly formed radicals continue to diffuse toward the substrate surface, when radicals collide with the surface there is a chance they will adsorb and react with it. These reactions are the steps that build up the diamond film. Unless deliberately altered, the final surface of diamond grown in this way will be comprised of 'dangling' hydrogen atoms.<sup>55</sup> Carbon can't be the terminating atom as it requires four covalent bonds to be stable, this wouldn't be possible as a surface atom. If a hydrogen radical collides with the surface there is a chance it will remove a dangling H atom from it; producing an  $H_2$  molecule. The resulting gap on the surface is a highly reactive site. Due to the higher concentration of hydrogen in the gas mixture, the site will typically react again with hydrogen and revert to its previous structure. There is, however, a slight chance that a methane radical will interact with the reactive site; irreversibly forming a carbon-carbon bond. These carbon-carbon bonds are the building steps that produce the diamond lattice.<sup>56</sup> Given enough time a tetrahedral carbon lattice will grow as unwanted graphitic carbon atoms are etched away.

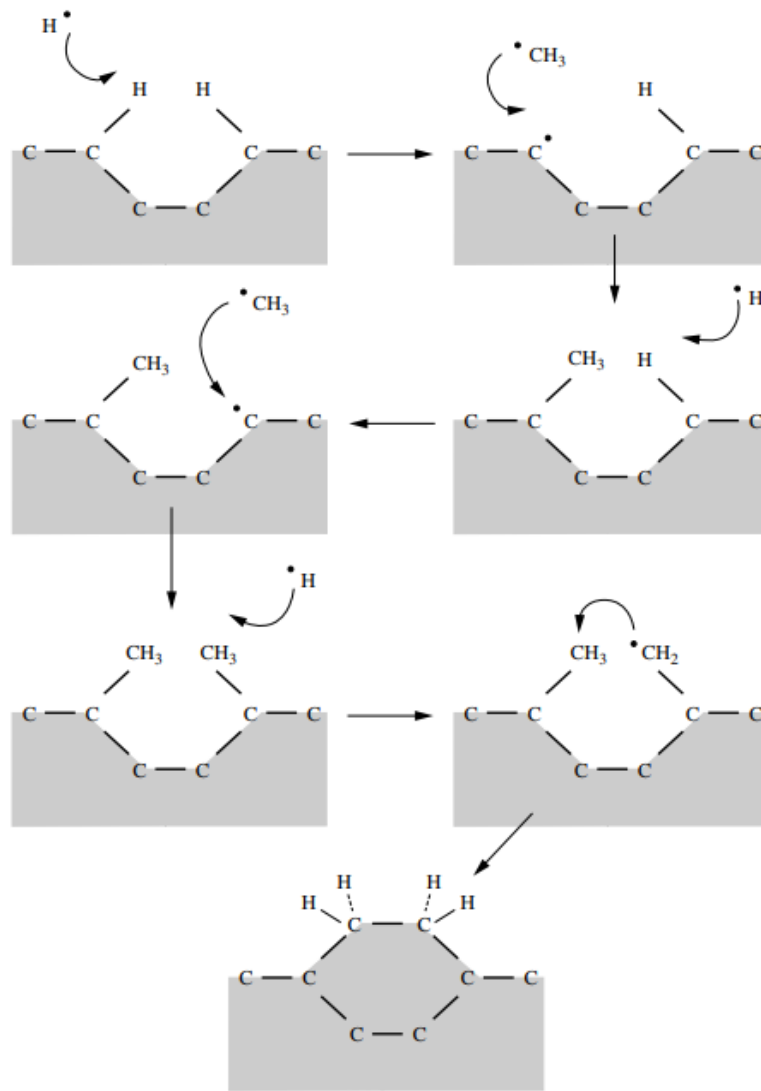


Figure 11. The reaction pathway which results in diamond growth, via the addition of highly reactive radicals to the surface of bulk diamond.<sup>56</sup>

### 1.4.1 Surface Termination

As mentioned above, the surface layer of diamond cannot be terminated by carbon due to the valency that would be required; in typical conditions CVD growth results in hydrogen termination of the film. This hydrogen termination is relatively unstable so can be replaced by other atoms or molecules. Changing the surface termination of diamond can alter the properties, for example certain groups affect the hydrophilicity of the surface.

Oxygen is commonly used to terminate the diamond surfaces; the process of doing so is relatively straightforward. As the carbon oxygen bonds produced are more thermodynamically stable than carbon hydrogen bonds, the replacement occurs over time if a hydrogen surface is exposed to air. Oxygen termination can also be achieved through exposure of the surface to oxygen plasma, or by dipping the sample into certain acid baths.<sup>57</sup> Amino terminated diamond surfaces can also be produced by exposing the surfaces to ammonia plasma.<sup>58</sup> In a very similar manner, fluorine termination can be achieved by using plasma of fluorine containing gases such as sulfur hexafluoride.<sup>59</sup>

Surface termination may affect the bactericidal properties of a material due to the affect it can have upon the surface wettability. More hydrophilic surfaces have been shown to increase rates of bacterial adhesion compared to hydrophobic surfaces. Considering bactericidal surfaces, it could be suggested that more adhesion is a good thing; more bacteria on the surface may result in a higher rate of cell destruction. This general trend of increasing cell adhesion is true for relatively flat surfaces but does not necessarily apply to the highly nanostructured surfaces being used in this research. In fact some work has shown that increasing hydrophobicity may actually increase adhesion to such surfaces.<sup>61</sup>

## 1.6 Previous Work

Significant work has been conducted regarding the bactericidal properties of black silicon. It has been shown to be effective against both gram-negative and gram-positive strains of bacteria, with higher death rates displayed by gram-negative strains. The bSi needles used in these studies were approximately 500 nm long, with a spacing of 200 nm.

Within the Bristol diamond group work has been undertaken looking into black diamond, and how a diamond coating affects the bactericidal properties of the material compared to bSi. The results of this work were promising, showing an increase in cell death by over 20% compared to a flat diamond control. The diamond coating did slightly decrease the cell death percentage when compared to bSi; this is thought to be caused by increasing tip diameter.

Different surface terminations have been carried out, and the resulting samples were also tested for their bactericidal properties. It was found that increasing the surface hydrophilicity, through oxygen termination, reduced the cell death percentage by almost 15 %, compared to an H-terminated sample.

All work done in Bristol has been using gram-negative bacteria, in particular *Escherichia coli*. This leaves a gap in the research as no gram-positive bacteria have yet been tested on black diamond surfaces.

## 1.7 Project Aims

The major aim of this work was to build upon the research that has previously been completed within the diamond group; to investigate the bactericidal properties of black silicon and black diamond. More specifically this work aimed to test how well such materials can be used to control the adhesion and growth of gram-positive bacteria; an area that has not yet been looked into. It also aimed to measure the effect that fluorine termination has upon the bactericidal properties of black diamond.

We hoped to achieve this by first fabricating black diamond using a range of bSi, ensuring the level of growth preserves the fine nanostructure. Half the samples would be fluorine terminated to test the effect this had. Bacterial testing will be carried out upon the samples, measuring the number of dead and alive cells after a short incubation, in live/dead assays.

As no work has been previously carried out using gram-positive bacteria, this work should set a foundation for future work in this area. It should provide an insight into what properties should be targeted for improving bactericidal properties and also what to be avoided.

## 2 Methodology

### 2.1 Sample Production

#### 2.1.1 Black Silicon, bSi

The first wafer of bSi used was produced by Colin Welch, from Oxford Instruments. A second wafer used was provided by Colin Welch. Before any additional processing, the wafers were cut into samples of size  $1\text{ cm}^2$ , using a diamond tipped scribe.

#### 2.1.2 Seeding

A seeding solution, consisting of 10 drops of NanoAmando colloid (particle size of  $3.3 \pm 0.6\text{ nm}$ , 2 % weight/volume in water), in 25 mL of methanol was produced; the solution was sonicated by a tip sonicator for 1 hour to ensure as little particle aggregation as possible. The bSi samples were attached to a rotating disk within the electrospray machine, using carbon sticky pads and the disk was rotated at 100 rpm. Approximately 5 mL of the seeding solution was added to a syringe connected to a high voltage power supply and a voltage of 65kV was applied to the needle. The solution flowed through the needle, depositing the nano-diamond onto the surface of the samples.

#### 2.1.3 Diamond Growth

The seeded bSi samples were put into HFCVD reactor, the reaction chamber was put under vacuum and allowed to reach  $<20\text{ mTorr}$ . The substrate heater was turned on and allowed to heat the sample for 20 minutes. Gas, with a composition of 1 % methane in hydrogen, was flowed into the chamber with a total flow rate of 200 sccm. A further 0.7 sccm of dilute diborane in hydrogen was flowed into the chamber. By changing the strength of the vacuum applied, the pressure of the chamber was adjusted to 20 Torr.

A current of 25 A was supplied to 3 Tantalum filaments, producing a voltage of  $\sim 9\text{ V}$ . The voltage increased with time as the filament began to degrade. The growth was run for the required time depending upon the sample; 20 minutes for  $2.4\text{ }\mu\text{m}$  needles and 15 minutes for  $2.7\text{ }\mu\text{m}$  samples. The methane and diborane gases were turned off 2 minutes before the end of the runs; this was to encourage full hydrogen termination.

#### 2.1.4 Termination

The samples requiring fluorine termination were placed into a DC plasma generating terminator, 4 at a time. The chamber was evacuated of air and argon was flowed through for 10 minutes, the chamber was pumped down to  $<10\text{ mTorr}$ .  $\text{SF}_6$  was flowed into the chamber and allowed to reach a pressure of 1 Torr, this was achieved by altering the vacuum being applied. A large voltage was applied to the sample tray, generating a fluorine plasma, this was done for 10 seconds.

## **2.2 Characterisation**

### **2.2.1 Scanning Electron Microscopy**

Samples were characterised via scanning electron microscopy (SEM), images were taken for further analysis of nano-structures.

### **2.2.2 Water Droplet Contact Angle**

Samples were loaded onto a Kruss droplet shape analyser, a syringe was filled with deionised water and put into the equipment, with the needle diameter measured for calibration. A droplet of water with volume 1.5  $\mu\text{L}$  was produced onto the surface. Using a side facing camera, the contact angle between the droplet and the surface was measured, using the Advance program; three measurements were carried out for each droplet.

### **2.2.3 Raman**

Raman spectra of the samples were collected using a Renishaw Raman Spectrometer. The laser had a 514 nm wavelength with a power of  $\sim 30$  mW. The spectra acquisitions were 6 seconds long with 10 accumulations for each sample.

## **2.3 Bacterial Testing**

### **2.3.1 Culture Production**

A preculture was made by suspending a colony of *Staphylococcus Aureus* ATCC 12600 in 10 mL of sterile tryptic soy broth (TSB) at 37 °C and 150 rpm for 14 hours. 200 mL of TSB was mixed with the preculture in a 1:20 dilution and incubated at 37 °C for 16 hours in a static incubator. The resulting cells were collected by centrifugation at 6500 rpm and washed with 10 mL phosphate buffer solution (PBS). This step was repeated once more. The cells were collected and re-suspended in PBS, sonicated and counted in a Burker-Tirk counting chamber. A final bacterial suspension of  $10^7$  CFU/mL was made in TSB.

### **2.3.2 Live/Dead Assay**

Before testing, all surfaces were rinsed with 70% ethanol and placed into a well plate. 2 mL of the suspension described above was added to each sample and the samples were incubated at 37 °C for 1 hour. The surfaces were gently washed in a container of PBS, by rinsing 5 times. Live/Dead<sup>®</sup> BacLight<sup>™</sup> bacterial viability stain was added to the sample wells and the sample were incubated at room temperature for 15 minutes in the dark. Samples were then transferred to wells containing PBS and were characterised via fluorescence microscopy.

### **2.3.3 CFU Count Assay**

Before testing all surfaces were rinsed with 70% ethanol and placed into a well plate. 2 mL of the suspension described above was added to each sample and the samples were incubated at 37 °C for 24 hours. Samples were removed and washed in PBS, twice. The washed samples were then sonicated for 5 minutes in 1 mL PBS to remove bacteria. The resulting PBS bacteria suspension was serially diluted in 10 fold steps and each level of solution was spread over a TSB agar plate. Plates were incubated overnight at 37 °C in a cell incubator and the number of colonies counted the next morning after 14 hours.

## 2.4 Black silicon production

Four 1 cm<sup>2</sup> pieces of flat silicon were layered with scotch tape in such a way that removing each piece would expose a new quarter, with one quarter always exposed. A masking solution was made, consisting of 10 drops of NanoAmando colloid (particle size of 3.3 ± 0.6 nm, 2 % weight/volume in water), in 25 mL of methanol; the solution was sonicated for 1 hour. This solution was serially diluted to produce three solutions of 25, 5 and 1 % relative concentrations. The samples, along with the stock solution of colloids, were loaded onto the rotating metal disk of the electrospray equipment and rotated at ~100 rpm. 5 mL of the stock solution was added to the syringe and a voltage of 65 kV applied to the needle. When the solution has all passed through the needle the samples were removed and a layer of tape removed, exposing another quarter of the sample. The above process was then repeated for the 25, 5 and 1 % solutions, in that order, removing a layer of tape each time. By the end of this each sample had a different mask concentration on each quarter.

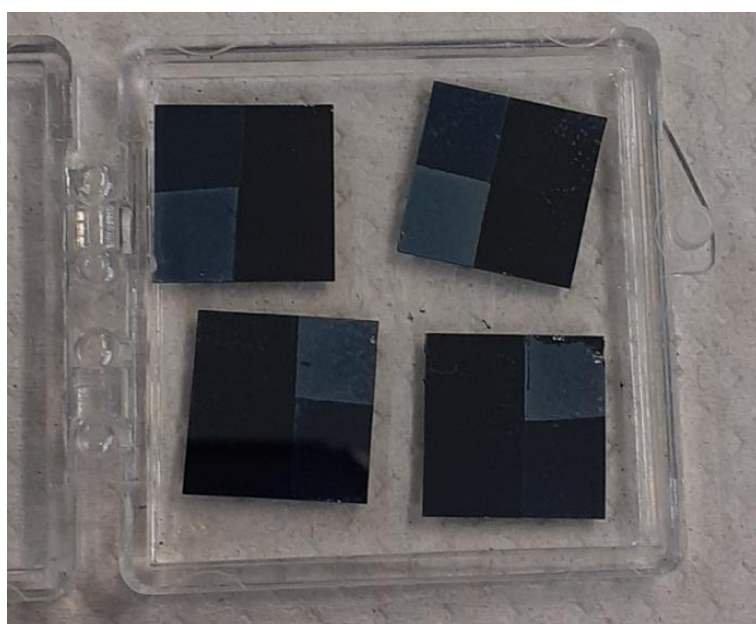


Figure 12. Silicon samples, each masked with nano-diamond, with a different masking concentration on each quarter.

The first of the samples was placed onto the substrate holder of the DC plasma generating terminator. In the same manner as described previously, a DC SF<sub>6</sub> plasma was generated. The sample was exposed to the plasma for 10 seconds. The next samples were exposed to the plasma for 1 minute, 5 minutes and 10 minutes; each with otherwise identical conditions.

## 3 Results and Discussion

### 3.1 Black Silicon

A number of bSi wafers were considered for use in the production of black diamond samples, each with different needle lengths and densities. The SEM images below show some of the potential samples.

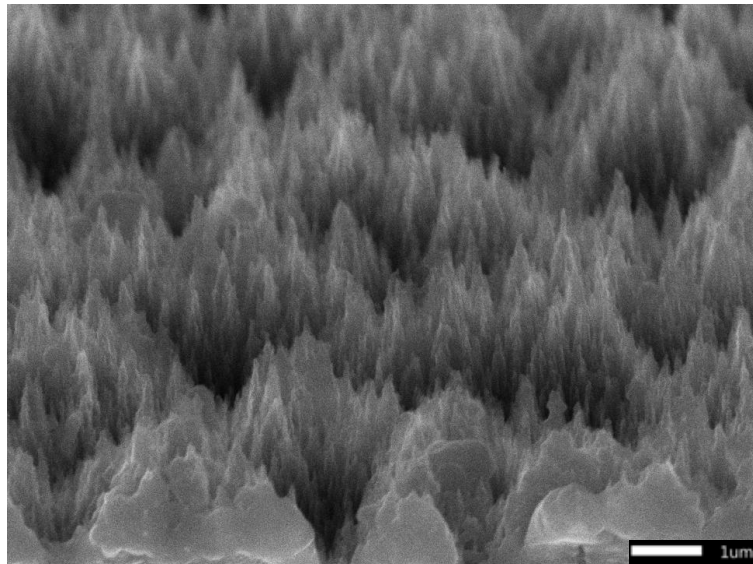


Figure 13. SEM image of a sample of bSi with average needle height of 1.3  $\mu\text{m}$ .

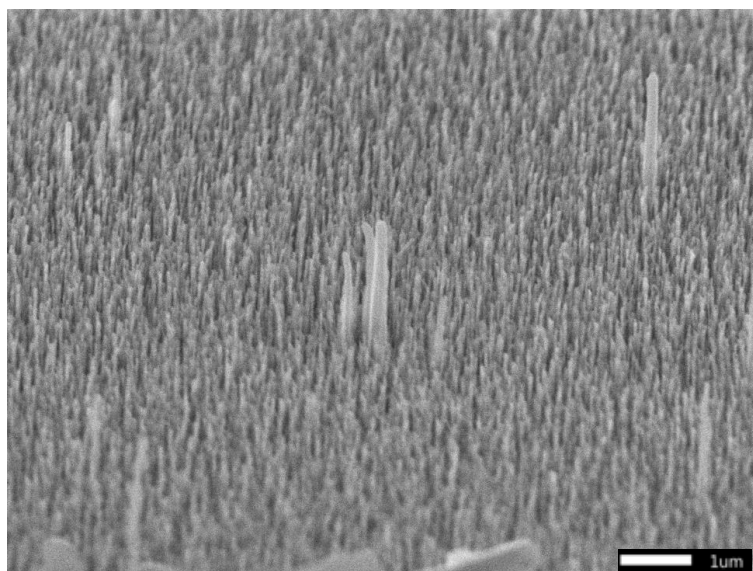


Figure 14. SEM image of a second sample of bSi, with an average needle height of 2.4  $\mu\text{m}$ .

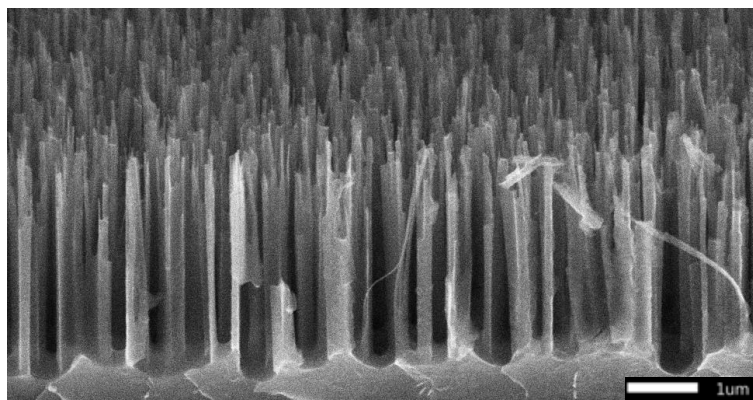


Figure 15. SEM image of a bSi sample with average needle length of 2.7 μm.

Due to their variety of needle lengths, shapes and densities, the three samples shown above were all used to produce a range of black diamond. The bSi shown in figure 13 can be seen to have more of a tipi peak shape, rather than the typical needle found in the other samples. It was thought that this change, alongside its varying peak heights, could be well suited to killing bacteria. Research showed that the wings of dragonflies are bactericidal toward both classes of bacteria; it is thought this is due to it possessing varying peak heights. The remaining two samples were chosen to be grown upon as similar bSi has previously been shown to be effective at killing certain bacteria; its ability to do the same to other strains is to be tested.

The bSi displayed in figures 14 and 15 have a needle spacing of approximately 300-400 nm, a similar scale to the structure of dragonfly wings, which have been found to be bactericidal toward gram-positive bacteria; this suggests that the bSi and resulting black diamond may be well suited to killing similar bacteria.

### 3.2 Black Diamond

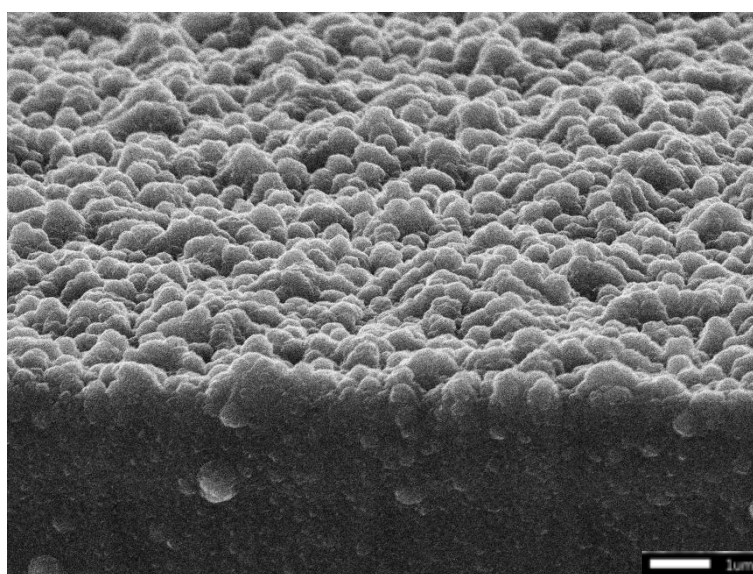


Figure 16. A sample of 1.3 μm needle bSi, after 1 hour of diamond growth.

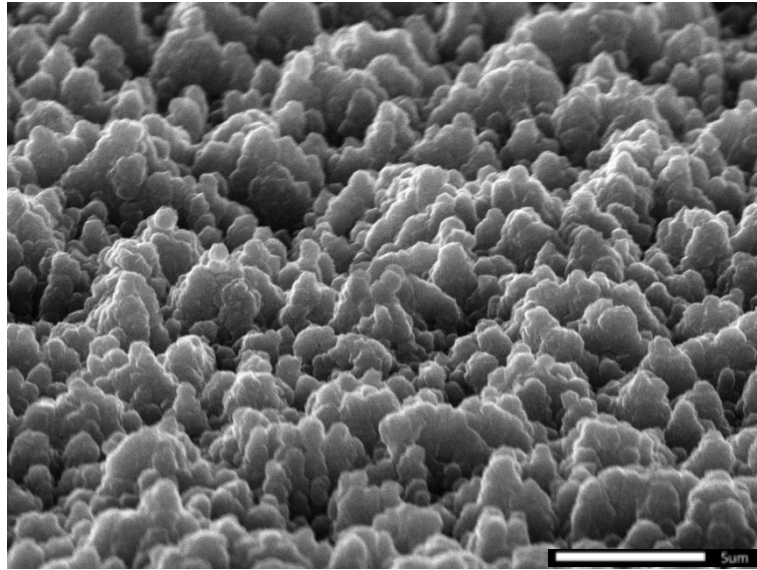


Figure 17. A sample of 1.3  $\mu\text{m}$  needle bSi, grown for 30 minutes.

Comparing figures 16 and 17 it can clearly be seen that the sample grown for only 30 minutes has retained much more of its original nano-structure, the peaks are more pronounced with much less growth in-between the individual tips. Considering the stretching mechanism of cell death that has been proposed previously, it would be expected that this preservation of surface structure would promote cell death. The cells have to be able to sink into the surface and adhere down the needles simultaneously; with shallower dips between peaks less stretching of cell membrane would be expected. Another key structural element to consider is the needle tip size, a wider tip would provide a better resting place for bacteria and could reduce the degree to which they attempt to sink into the surface. With both these points in mind, the shorter growth time was decided to be most suitable.

After considering the size and shape of the bacteria that will be used in this experiment, it was decided that the 1.3  $\mu\text{m}$  tipi bSi would ultimately not be suitable for the experiment. The first factor that led to this decision was the spacing of needles being too high, the bacteria to be used in this experiment was to be gram-positive, with typical cell diameter of  $\sim 1 \mu\text{m}$ . From figure 17, it can be deduced that in many places on the surface a bacterial cell of that size would nestle safely between peaks. If this were to occur, cell stretching would not take place, thus allowing the bacteria to proliferate on the surface. Another issue was that a good portion of the surface's fine structure was lost in the growth process, in figure 13 the tipi peaks are comprised of a large number of smaller peaks. This was part of the reason this bSi was chosen, in the black diamond sample many of these peaks have rounded out, in the process forming one larger peak.

bSi with 2.4  $\mu\text{m}$  needles was then investigated, three different diamond growth lengths were attempted, 20 minutes, 40 minutes and an hour. Two of the resulting surfaces are pictured below, the hour growth is not included as the peaks were barely visible due to overgrowth.

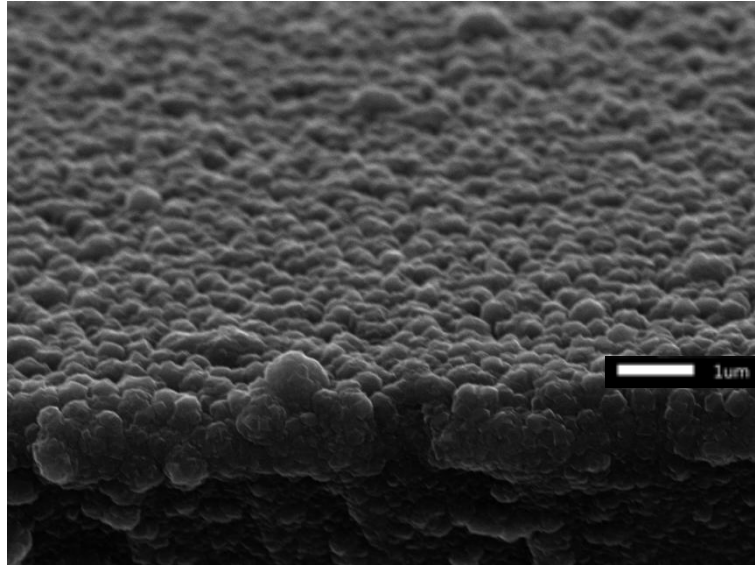


Figure 18. 2.4 μm bSi, after 40 minutes of diamond growth.

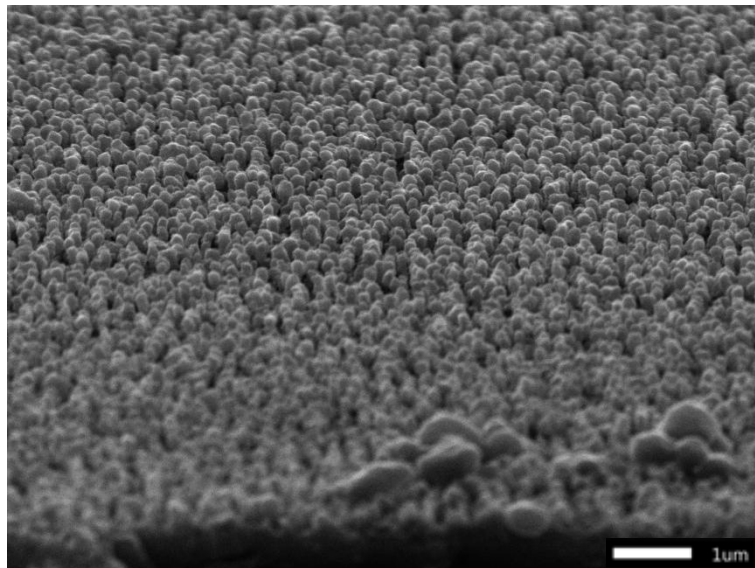


Figure 19. 2.4 μm bSi, after 20 minutes of diamond growth.

Looking at figure 18 and 19 above, it is clear that after 20 minutes of growth a much larger degree of the nanostructure is preserved. Much fewer of the needles have clumped and filled the troughs between them, leaving the gaps required for the bactericidal action. On the 40 minute sample the needles have also rounded out to a greater degree, increasing the needle tip diameter; this is expected to decrease the bactericidal properties. With this in mind, 20 minutes was selected as the optimum growth time as it provided a full coating on the needles whilst minimising loss of fine structure. Looking back at the tipi peaks it is clear that the needles have a more defined point and better spacing; two properties likely to increase the cell death rate. Once the growth length had been decided a full set of 16 identical samples was produced.

After this first set of samples had been tested for bacterial testing, a new wafer of bSi, with an average needle length of  $2.7\ \mu\text{m}$  was acquired (Fig. 15). Based on growth times used for the previous bSi, initially 20 minutes of diamond growth was carried out on the sample. An SEM image of this is shown below (Fig. 20). Although the surface is fully coated in diamond, there are some areas in which the needles have been overgrown and clumped together. Knowing the effect this may have upon the bactericidal properties a 15 minute growth was carried out.

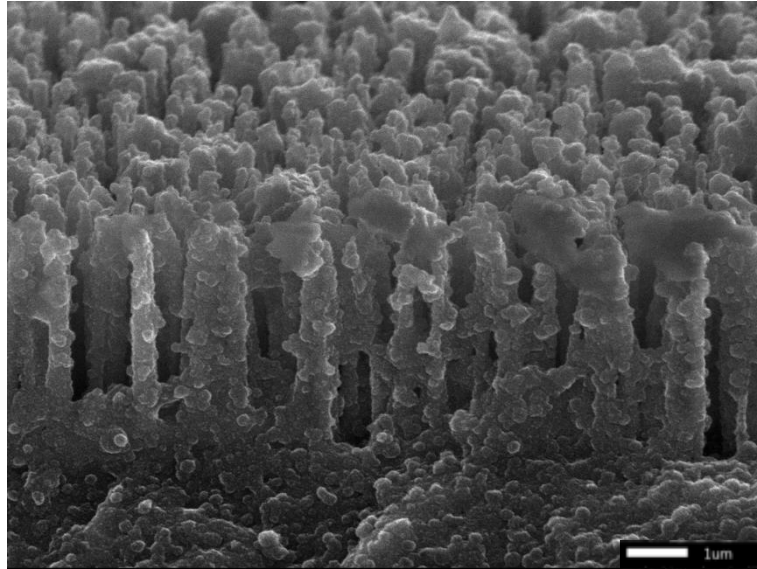


Figure 20.  $2.7\ \mu\text{m}$  bSi, after 20 minutes of diamond growth.

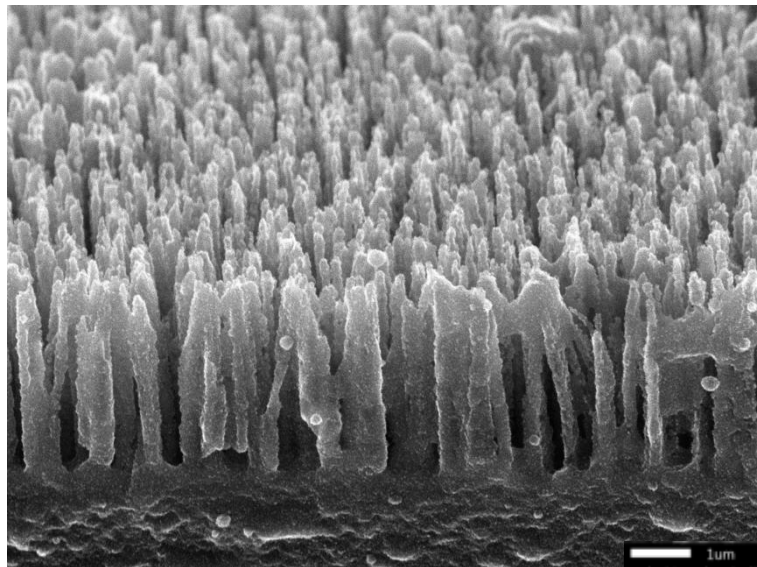


Figure 21.  $2.7\ \mu\text{m}$  bSi, after 15 minutes of diamond growth.

In figure 21, in the bulk of the surface the needles are far better separated; based on the proposed cell death mechanism this should improve the surface's bactericidal properties. Another key difference between the two growth lengths is the needle tip diameter; figure 21 displays a noticeably smaller tip. This factor will also likely improve the bactericidal properties.

### 3.3 Water Droplet Contact Angle

Sample	Termination	Water drop contact angle / degrees
2.4µm bSi	H	-
	F	-
2.4 µm bDia	H	81.3
	F	-
2.7 µm bSi	H	112.2
	F	-
2.7 µm bDia	H	68.7
	F	-

Complete wetting of the droplet onto the surface was observed for five samples, the four fluorine terminated surfaces and the 2.4 µm bSi sample, in each case the droplet touched the surface and instantly lost its shape. This meant no contact angle could be observed or measured. All of the fluorine terminated samples gave the same complete wetting outcome; this suggested that this polar surface bond reduces the sample's hydrophobicity. This was not the expected result as fluorine termination typically increases hydrophobicity. The combination of fluorine termination and the nanostructure of the surface must, in some way, interfere with the surface tension. No surface tension results in a loss of droplet shape and therefore surface wetting.

Interestingly, the hydrogen terminated sample of: 2.7 µm bSi, 2.7 µm bDiamond, and 2.4 µm bDiamond were all able to give reliable results. A surface is classified as hydrophobic if the water droplet contact angle is over 90°, making only the 2.7 µm bSi hydrophobic. This was likely due to a combination of its surface properties, one potential explanation being the hydrogen termination preventing the nanostructure from interfering with surface tension; stopping surface wetting from occurring. For this to be the case there would have to be another difference between the H-terminated 2.7 µm bSi and bDiamond, to cause the difference in hydrophobicity. A possible differing property is the needle tip size; with no diamond growth the tip diameter is much smaller in the bSi sample. The water droplet may sit atop the smaller needles more easily, resulting in higher contact angles.

The 2.4 µm bDiamond sample was shown to be slightly hydrophilic with a contact angle of 81.3. This is most likely due to similar reasons as mentioned above for the 2.7 µm needles. However, the above explanation doesn't fully explain these results as the 2.4 µm bSi resulted in complete wetting of the surface, therefore in this case the smaller needle tip did not increase hydrophobicity.

With this in mind it should be said that the explanations given above are hypotheses that attempt to make sense of the data that was available. To be sure of any of this reasoning more experimental data would be required. Firstly, more samples of bSi should be tested, with careful note of the needle tip size. Another property to consider is the density of the needles, as this would affect how the water droplet sits upon the surface. A greater range of surface terminations should also be investigated, looking into terminations such as oxygen, which is expected to increase hydrophilicity rather than decrease like fluorine.

Sample	Termination	Water drop contact angle
Flat Silicon	H	31.2
	F	61.1
Flat Diamond	H	98.9
	F	86.4

After the interesting results found with the nanostructured surfaces, control tests were carried out upon flat samples. These were performed to ensure the fluorine terminations were successfully depositing fluorine on the surfaces. A polished surface of silicon was the first to be tested on in this manner. Reassuringly, the water contact angle almost doubled from 31.2° to 61.1°; this shows a drastic increase in hydrophobicity and revealed that the termination had been successful. Next, a flat sample of diamond was tested, here the contact angle decreased slightly after fluorine termination. The decrease is relatively small and can be explained by the roughness of the surface. Unlike the polished silicon surface, the diamond contained many imperfections and grain boundaries; these probably affected the terminations effectiveness.

### 3.4 Raman

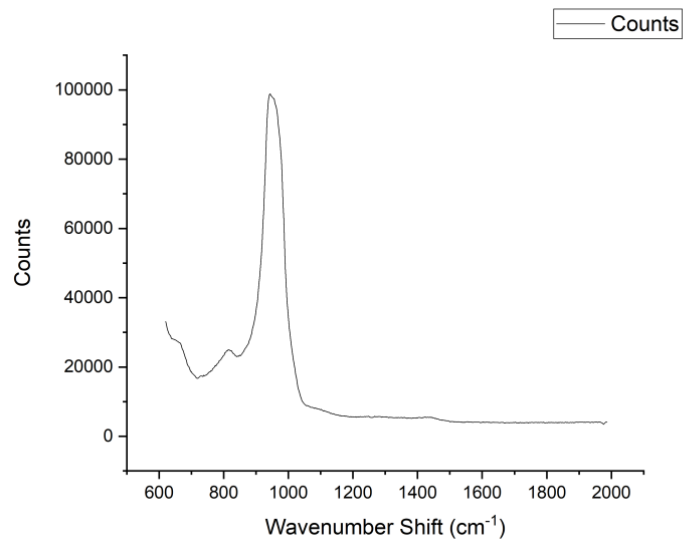


Figure 22. Raman spectrum of uncoated bSi, with 2.4 μm needles.

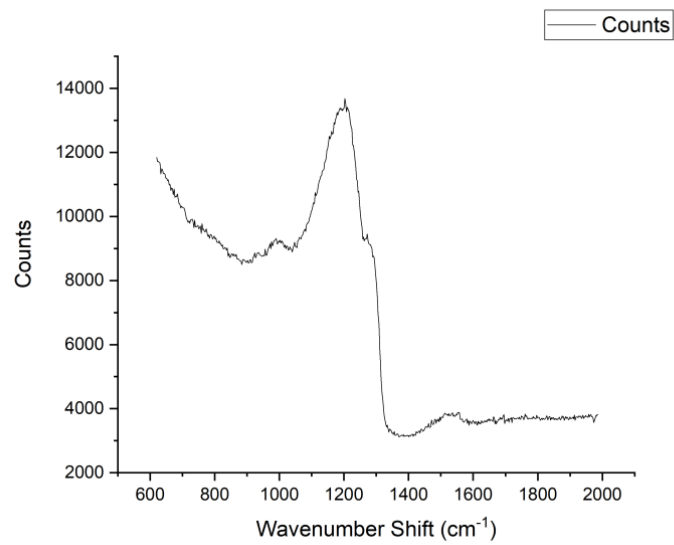


Figure 23. Raman spectrum of 2.4 μm bSi after 20 minutes of diamond growth.

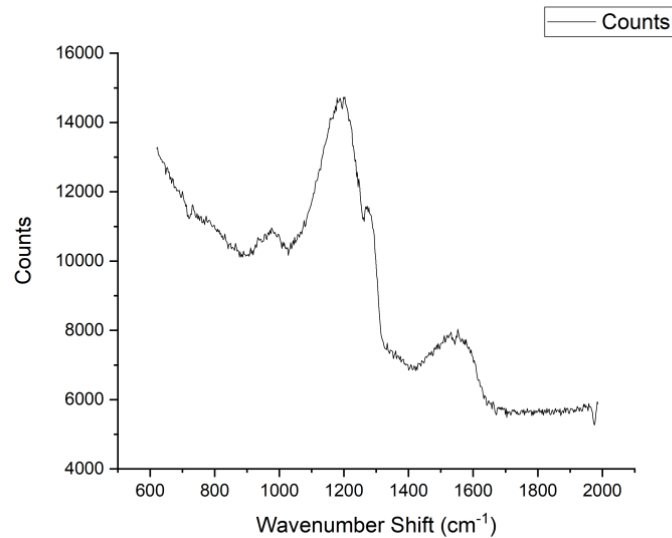


Figure 24. Raman spectrum of 2.7  $\mu\text{m}$  bSi after 15 minutes of diamond growth.

Silicon typically shows a peak in a Raman spectrum at about  $520\text{ cm}^{-1}$ , this peak has been cropped from figure 22 to allow the other peaks to be seen, as the first order peak has a very high intensity. The removal of this peak also allows for continuity between the other spectra. The peak seen at  $950\text{ cm}^{-1}$  can also be attributed to silicon and has been reported in literature to appear in the Raman spectrum of nanostructured silicon.<sup>60</sup>

Diamond displays a peak at  $1332\text{ cm}^{-1}$  in a typical Raman spectrum; looking at both figure 23 and 24 it can be seen that such a peak is missing. This is, at first, unexpected as we have grown a layer of diamond upon each of these samples so would expect to see this peak. However, this peak isn't detected due to the crystal size of the diamond that is present. Smaller crystals, in this case nano-diamond, result in peaks that are shifted to lower wavenumbers. This is reported throughout the literature, with peak typically found at  $1100\text{-}1200\text{ cm}^{-1}$  dependent upon crystal size.

Considering the growth conditions of these samples it becomes clear why such peaks were observed. The samples were seeded with a nano-diamond solution, and the growth times were relatively short, resulting in the crystals within the diamond layer remaining relatively small. These nano-crystals can be seen in the SEM images (figures 16-21) of the black diamond samples.

A final point to note is the clear difference between the spectra of the bSi and the bDiamond, suggesting that the surface composition has been drastically changed. The large peak at  $950\text{ cm}^{-1}$  is no longer present in the bDiamond spectra, and the peak at  $1150\text{ cm}^{-1}$  can't be seen in the bSi spectrum.

### 3.5 Black silicon fabrication

From initial inspection of the samples it was clear the required specifications had not been fully achieved. The samples did not have the deep black colour that can be seen in other pieces of black silicon, there was however a slight colour change within some of the samples, the polished finish was lost and the colour changed from silver to an off white.

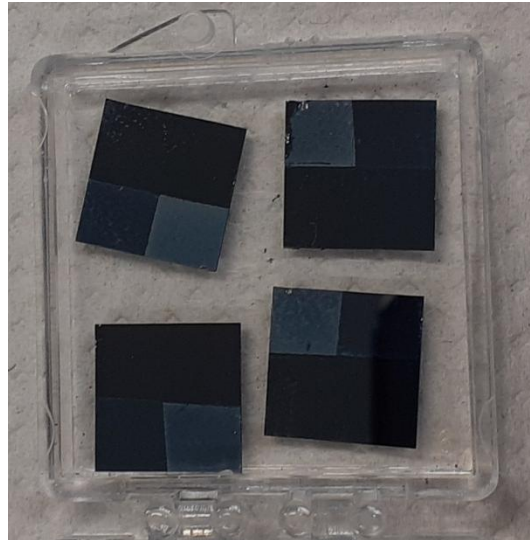


Figure 25. Masked silicon wafers, before etching.

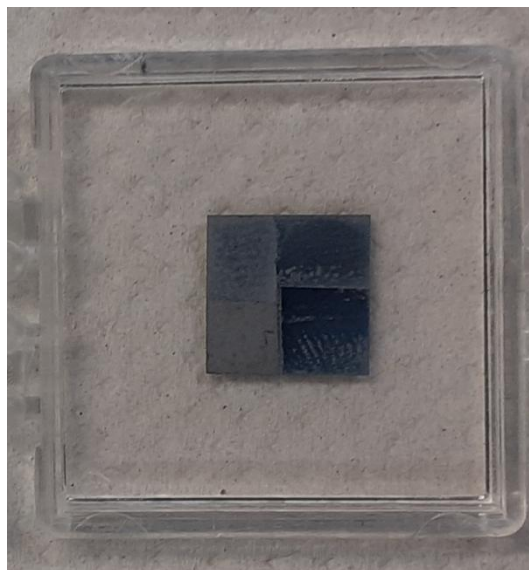


Figure 26. A sample after 5 minutes of plasma etching.

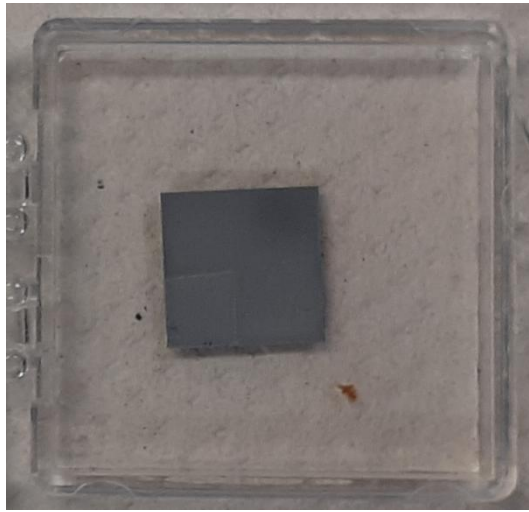


Figure 27. A sample after 10 minute of plasma etching.

Images of the sample that were etched for 10 seconds and a minute are not included here as they are almost identical as to before any etching. From these images alone very little can be deduced and so the samples wer analysed by SEM, the data from which are shown below.

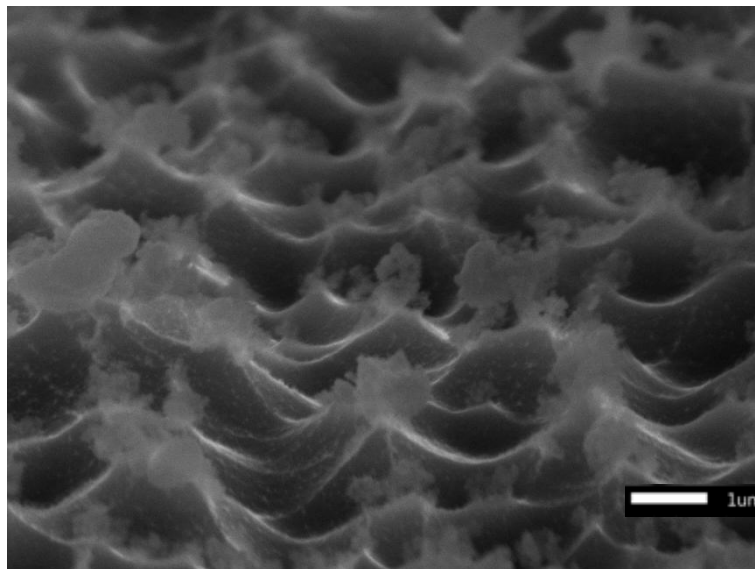


Figure 28. SEM image of the silicon sample with a 131 % relative masking concentration, after ten minutes of etching.

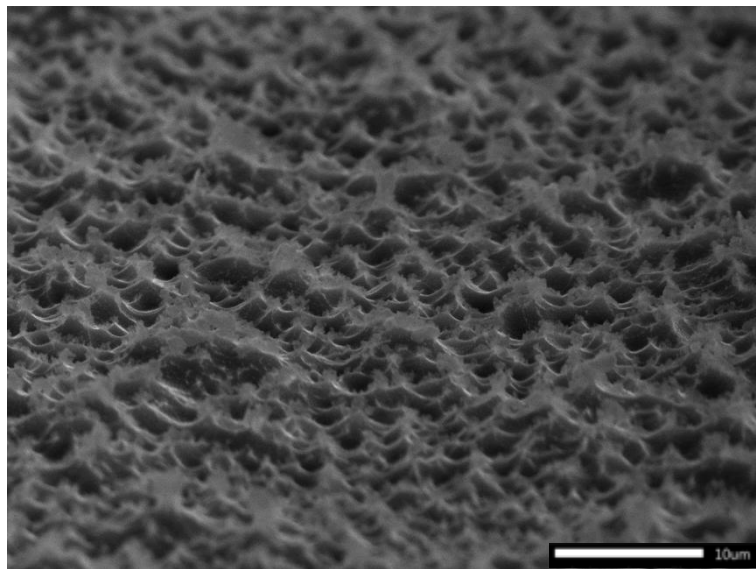


Figure 29. SEM image of the silicon sample with a 131 % relative masking concentration, after ten minutes of etching.

The two figures above show one of the best surfaces that was fabricated using the procedure outlined above. It is clear to see that some etching has occurred as the surface is no longer a flat polished surface; this reassures that the  $\text{SF}_6$  plasma had been generated successfully. Looking in more detail, it can be seen that the peaks on the surface of this sample are unfortunately not particularly needle like, possessing more of a tipi structure. Whilst some of the bSi previously worked with did have a similar structure, it was deemed unsuitable for the bactericidal application of this experiment. The two images also show a certain number of residual diamond particles on the surface, these would need to be removed before the samples could be processed any further.

More importantly, we must consider the scale of the structural elements on the surface. The peaks in this sample are up to 1 micron thick, with peak to peak separations up to several microns in length. Considering the size of the bacteria in question ( $\sim 1$  micron), and the mechanism of cell death, it is very likely that the surface would not be capable of killing bacteria. It is more likely that any bacteria to adhere to the surface would rest between the peaks with no membrane stretching occurring. This is before considering a diamond coating, which has been consistently shown to reduce cell death rates.

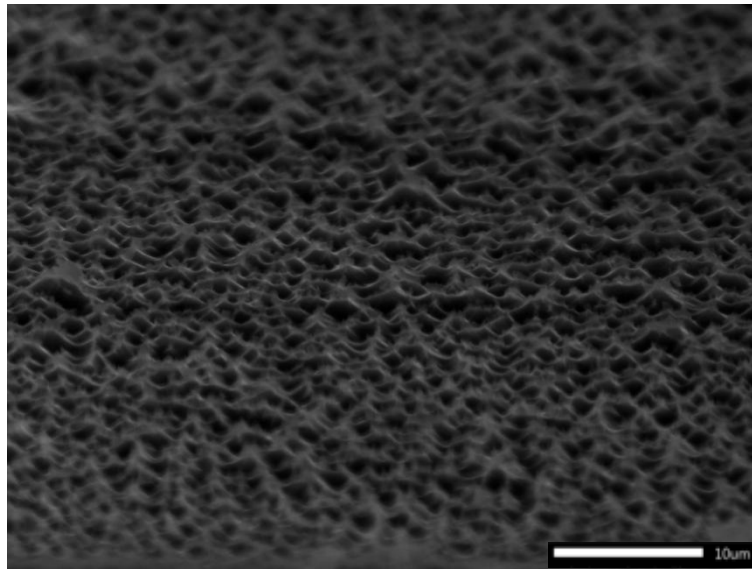


Figure 30. SEM image of the silicon sample with a 1 % relative masking concentration, after ten minutes of etching.

Interestingly, the surface of the sample shown above has a very similar peak density to the sample with much higher masking concentration. This test was conducted with the thought that the masking density would determine the density of peaks, as only the silicon under diamond particles would have been protected from the plasma. This result suggests that perhaps the mask that was applied does not actually affect the etching rates and there is a different etching mechanism producing the peaks observed.

Just like the previous sample, the aspect ratio of the peaks is too low, with a tipi structure rather than the desired needles. The consistency in shape between the two does again suggest the mask is not responsible for the nanostructure we are seeing.

After further research into the fabrication of black silicon it was observed that changing the gas composition within the chamber altered the way the plasma etches. To achieve the needle structure, the plasma composition will need to be altered, adding small concentrations of dopant gases to the mixture.

## 3.6 Bactericidal Results

### 3.6.1 Cell Death Percentages

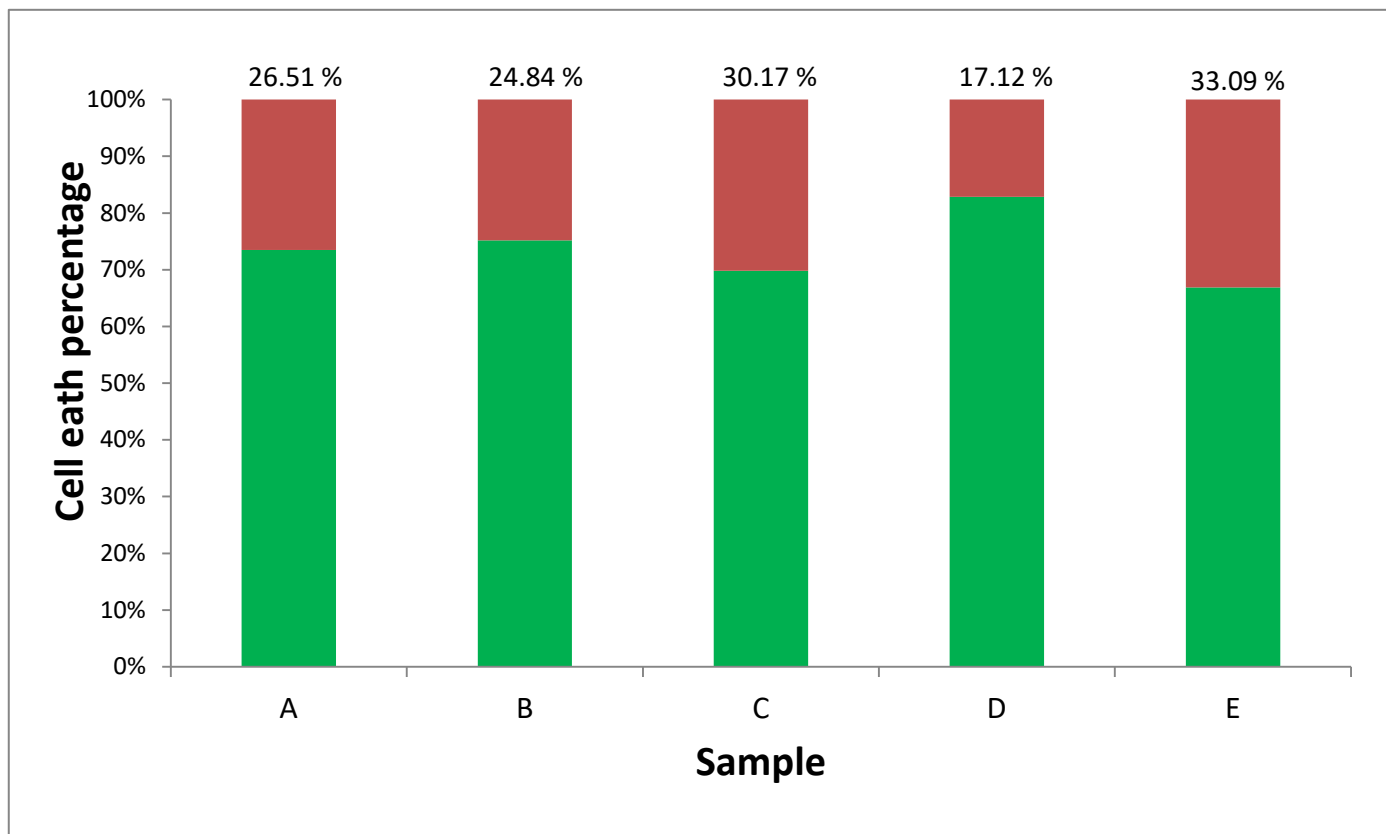


Figure 31. A graph displaying the cell death percentages of a range of samples.

Label	Sample Description
A	F-terminated flat diamond
B	F-terminated black diamond
C	H-terminated flat diamond
D	H-terminated black diamond
E	Black silicon

The first results to look at are those for samples A and B, the two fluorine terminated samples; it has been found that the flat diamond control actually had a slightly higher cell death percentage than the black diamond sample. It should be noted that the difference is very small and would very likely be found to be insignificant with more repeats, however this was limited in this first run of testing due to time constraints. This result is, of course, unexpected as the needles have been previously shown to improve cell death rates but again further work would have to be performed to show that this result is significant. However, previous work in this area has focussed only on gram-negative bacteria so there was a certain amount of uncertainty regarding how effective the surfaces would be against gram-positive bacteria.

With samples C and D, a similar trend is seen, with the flat diamond control having a higher cell death percentage. The difference between the two results is larger and more significant, with almost a halving in cell death percentage. Again these results are unexpected and will need to be repeated to ensure reproducibility.

Comparing the two black diamond samples, B and D, fluorine termination affords a higher cell death percentage. Considering this, it could be argued that fluorine termination has improved the bactericidal properties of the sample. Despite this increase, it cannot be ignored that the flat samples were both shown to have better bactericidal properties. This limits any possible applications of black diamond as a bactericidal surface, at least in places where gram-positive bacteria are present.

The result for sample E, an uncoated piece of bSi, provides the highest cell death percentage of the whole set. The result is only a few percent higher than the other samples, but it does suggest a more efficient killing surface. To improve cell death percentages in the future, it appears, as expected, the fine nanostructure of the bSi should be preserved as much as possible. This could mean finding ways to decrease tip diameters for example. As covered in the introduction decreasing tip size has been linked to an improvement of bactericidal properties in the wings of dragonflies; this should extend to black diamond surfaces.

Whilst analysing the results above, it needs to be mentioned that the testing was not carried out in an ideal fashion. The ability to perform repeats was severely limited, with samples only able to be used once. We expected the flat samples to be reusable after cleaning but with the cleaning methods attempted, this was not found to be the case. A larger number of the black diamond samples were sent for testing, however multiple were damaged in transport. Time constraints also played a part in the limited testing, with many samples being left unused. At this current time, data from only one repeat of each sample was available. This lack of repeats means no concrete conclusions can be drawn, at least not with high certainty.

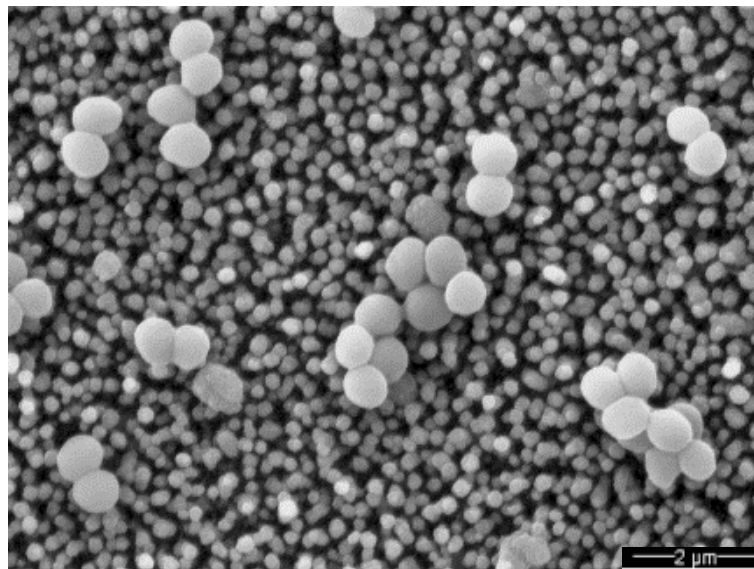


Figure 32. An SEM image showing bacteria on the black diamond needles of sample D.

In order to better understand the results of this testing, SEM images of the surfaces were taken, after an hour of incubation at 37 °C. In figure 32 above, the bacteria can clearly be seen upon the surface of sample, with the majority fully intact. This is as expected as the cell death percentage for this particular sample was only 17%. The important thing to note is that the bacteria appear to be

sitting atop the needles, rather than adhering down the needles and into the surface. This adhesion down the needles is required for the mechanism of cell death to occur. This image shows us that the structure of these samples is not suitable for this strain of bacteria; this is not to say that they may not be suitable for use with other strains. It is expected that these smaller sized bacteria will require more densely packed needles as the bacteria must be able to come into contact with several at a time for the stretching to occur. This idea of many points of contact was suggested by Kelleher when he investigated the wings of several cicada species.<sup>36</sup> Smaller needle tips will most likely be more suited to these bacteria for a similar reason.

### 3.6.2 Number of adhered cells

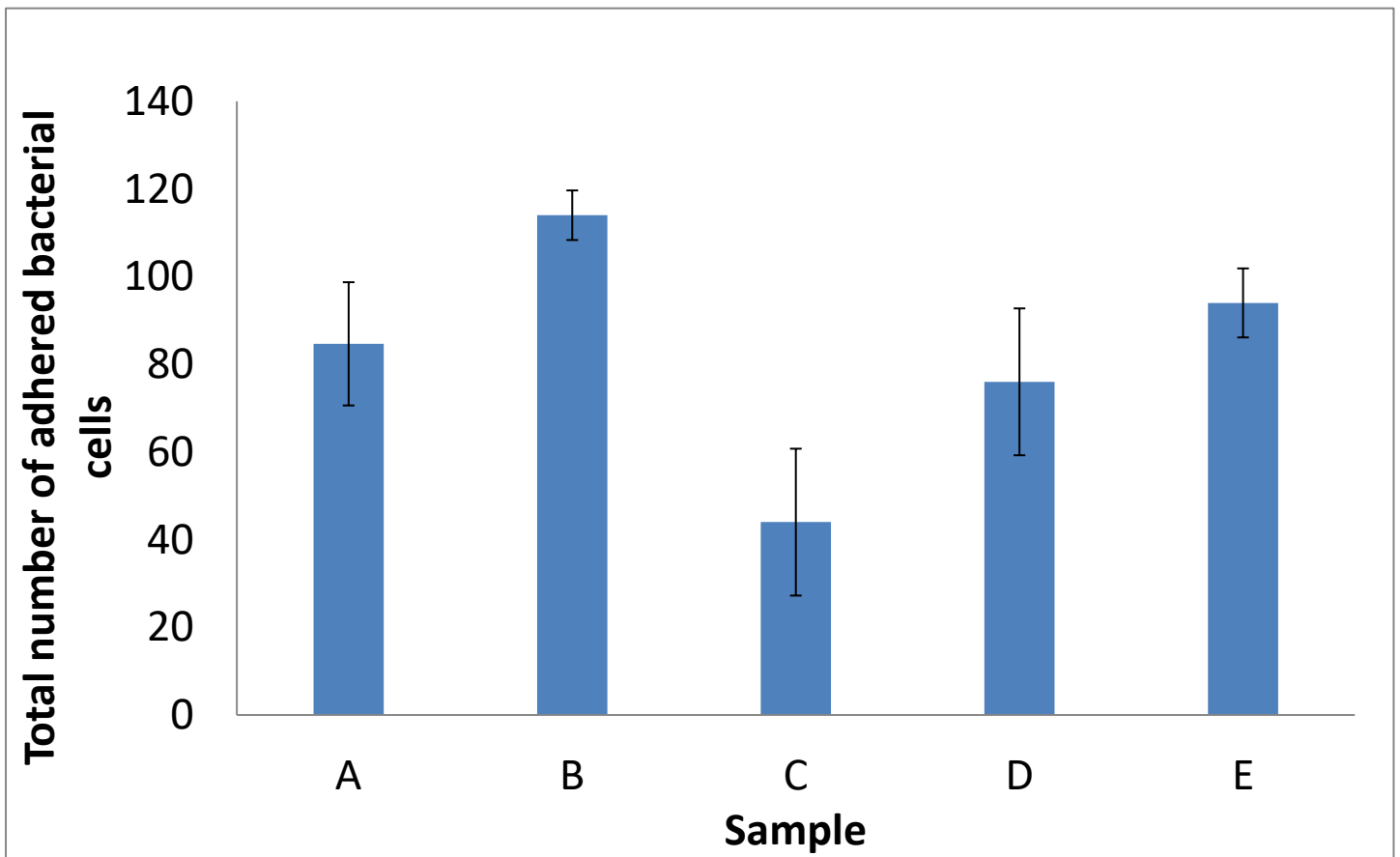


Figure 33. A graph displaying the total number of adhered cells to each sample, after one hour of incubation.

Label	Sample Description
A	F-terminated flat diamond
B	F-terminated black diamond
C	H-terminated flat diamond
D	H-terminated black diamond
E	Black silicon

Comparing the fluorine terminated samples to the hydrogen terminated ones, it can be seen that the fluorine terminated had a higher number of adhered cells, when comparing the similarly structured samples (A compared to C, and B with D). This suggests that the fluorine on the surface of the sample creates a stronger attraction between it and the cell. The polar surface bonds likely have a favourable interaction with the bacterial binding proteins; which are employed by cells to adhere to surfaces. This is also found to be the case in other work surrounding highly nanostructured materials.<sup>61</sup>

Another point to note is that the black diamond samples both have a higher number of adhered cells than their flat controls with the same surface termination. Knowing the samples are otherwise identical it can be assumed that the surface structure is responsible for this difference. In literature surrounding this area, it has been shown that bacteria adhere more favourably to rougher surfaces; this follows in the results above as the nano-structured black diamond is the rougher of the two samples.

There are some points of concern when considering this data, the first being that there is no way of knowing the percentage of cells that are adhering. To enable this, the total number of cells that come into contact with the surface would also have to be recorded; this would be a very difficult task with no straightforward solutions. Having this data would shed a light onto how favourable interactions between surfaces and bacteria actually are. Without knowing that the same number of cells came into contact with each surface, we cannot be confident that the fluorine surfaces are actually adhered to at a higher rate, just that a higher number have.

As with the data for cell death percentages, the lack of a good number of repeats reduces the confidence in any conclusions that are drawn. This uncertainty is also displayed here by the large error bars that are displayed on the graph. In many cases the differences between two results are largely eliminated by the error bars, meaning the results are very possibly not significantly different. For example samples C and D, the error bars for these two samples are overlapping so concluding that there is any real difference between the two is a weak conclusion at best. Of course, with more repeats the errors may reduce which would allow for an increased level of confidence in the data. Ideally a greater number of repeats would have been carried out, but again the issues with cleaning the samples and time constraints did not allow this.

When moving forward with this work, fluorine termination should be considered as a method of increasing the cell adhesion. However, considering the limitations of the current data, a wider number of samples should be tested to ensure the validity of this idea. In the scope of this work increasing cell adhesion numbers would be beneficial as the mechanism of cell death requires bacteria to fully adhere to the surface before death occurs.

### 3.6.3 CFU Counts

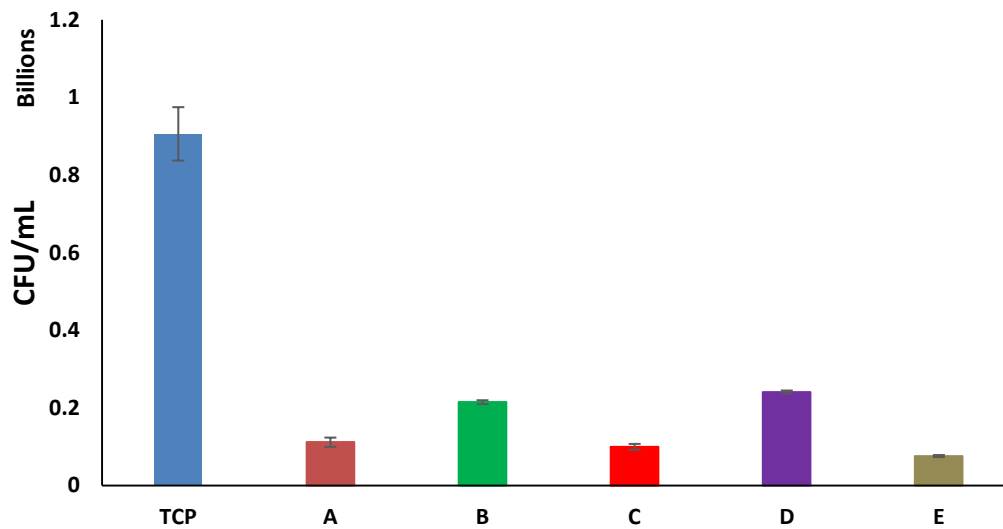


Figure 34. A graph displaying the results of a CFU count assay, after 24 hours of incubation at 37 °C.

The graph above shows that even after an ethanol rinse each of the samples still contained a large number of bacterial cells that are capable of multiplying and forming a bacterial colony. This tells us that the samples are not able to be reliably tested upon more than once as the bacteria that are retained from previous tests will interfere with results. It can be seen that sample B and D had a higher number of CFU's compared to the flat controls, suggesting that the bacteria adhered more strongly to the nano-structured surfaces. More vigorous methods of cleaning could be employed but doing so runs the risk of damaging the needles, even with the added strength the diamond provides.

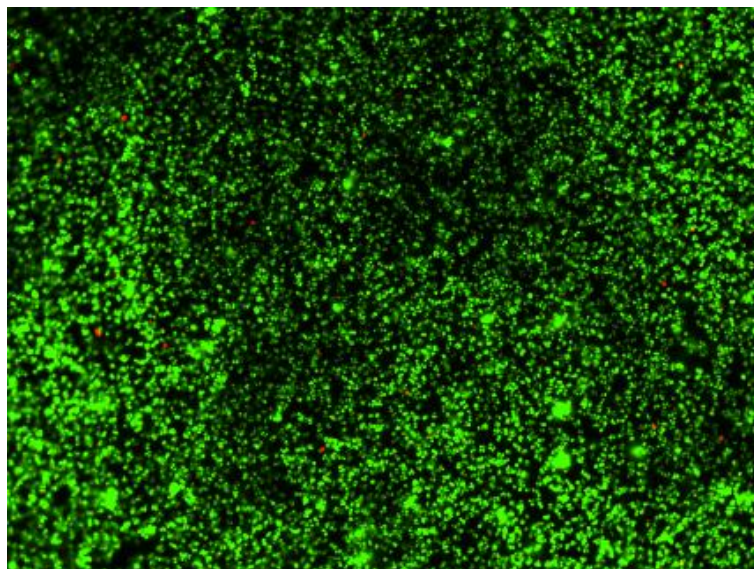


Figure 35. A fluorescence microscopy image of sample B after 5 hours of incubation at 37 °C.

This image displays the surfaces inability to inhibit the growth of bacteria that have adhered to the surface as there are very few dead cells compared the large number of living cells. This suggests that although the surface may be able to kill a certain percentage of cells that adhere, once a cell begins to replicate the surface does very little to slow this process down. This issue would make such surfaces of little use in many applications as they will not stop bacterial proliferation and biofilm formation.

## 4 Conclusion

Firstly, the black diamond grown from the 2.4  $\mu\text{m}$  needle bSi has been shown to not be an effective bactericidal surface towards *staphylococcus aureus*, a gram-positive bacteria. The flat diamond controls used in this work resulted in a higher percentage of cell death than black diamond. However, the surface that was produced may be effective against other gram-positive bacteria; this would likely depend upon the cell size and shape. The cell would likely need to make contact with more needles so perhaps larger cells would be killed by the surface. Based upon previous work, the needles would probably be effective against gram-negative bacteria but this would need to be tested.

Fluorine termination marginally improved the surfaces bactericidal properties of the surfaces as the F-terminated black diamond sample had a slightly higher cell death percentage. Considering that the flat diamond controls had higher cell death, this may have little use with these specific samples; this could still be applied in any further work however. Fluorine termination was also shown to increase cell adhesion to the black diamond; this fact may prove useful in future work. The data regarding cell adhesion is of limited confidence as no value for the total number of cells coming into contact with the surface was recorded. Due to a lack of data, the above conclusions must be considered critically, as there is no way to be sure of the repeatability of results.

Lastly, the fabrication method of black silicon attempted in this work was unsuccessful, producing surface protrusions that were both the wrong structure and size. More fine-tuning of the etching process will be required to produce the nano-needles that were aimed for. However, there is confidence that the plasma generated was capable of etching silicon, and an exposure time of ten minutes should be suitable to generate the needle height required.

## 5 Future work

The first and most important next step will be to perform more repeats on the samples that have already been produced. There is an entire new set of samples ready for bacterial testing, and several of the 2.4  $\mu\text{m}$  black diamond samples that can be used as repeats. These repeats would allow for greater levels of confidence in the results; they may even result in new conclusions as the data is analysed.

Building on from this, a greater range of black silicon should be tested upon, with different needle heights and densities. I believe that the most important property to look at will be the density of the needles as this determines how many needles each bacteria will come into contact with; this is also affected by the needle tip diameter. Research into naturally occurring bactericidal surfaces has shown that the wings of certain dragon fly are bactericidal towards gram-positive bacteria. It is thought that this is due to the varied heights of the peaks on the wing. Considering this, I suggest that bSi with varying needle heights on the same sample should be tested for a surface that is bactericidal toward gram-positive bacteria.

The samples produced in this work should also be tested against different strains of bacteria, both gram-positive and gram-negative. The efficiency of the surfaces will of course be affected by the structure of the bacteria itself. I expect that larger cells (i.e. gram-negative and certain gram-positive) will be effectively killed by the surfaces that have been produced, as enough of the needles will make contact with the cell membrane.

Lastly, a new area of research to be looked at is how well, and if at all, black diamond surfaces can be used to control algae adherence and growth. With such a large biodiversity within algae I expect it will be exceedingly difficult to find a surface that is suitable for all applications. This project has shown how difficult this can be when working between the two classes of bacteria. However, algae similar in size and structure to bacterial cells are likely to be susceptible to the mechanism of cell death that is employed by black diamond.

## Bibliography

1. T. Stanton, *Trends in Microbiology*, 2013, **21**, 111-113.
2. 2.R. Donlan, *Clinical Infectious Diseases*, 2001, **33**, 1387-1392.
3. 3.I. Williams, W. Venables, D. Lloyd, F. Paul and I. Critchley, *Microbiology*, 1997, **143**, 2407-2413.
4. H. Ceri, M. E. Olson, C. Stremick, R. R. Read, D. Morck, A. Buret, *J. of Clinical Microbiology*, 1999, **37(6)**, 1771-1776
5. S. Veerachamy, T. Yarlagadda, G. Manivasagam and P. Yarlagadda, *Proceedings of the Institution of Mechanical Engineers, Part H: Journal of Engineering in Medicine*, 2014, **228**, 1083-1099.
6. G. D. Ehrlich, F. Z. Hu, Q. Lin, W. Costerton, J. C. Post, *ASM News*, 2004, **70(3)**, 127-133.
7. J. Kwiecinski, *Letters in Applied Microbiology*, 2015, **61**, 511-517.
8. B. Meyer, *International Biodeterioration & Biodegradation*, 2003, **51**, 249-253.
9. Haak, P. W., *Proceedings of the International One-day Symposium on Antifouling Paints for Ocean-going Vessels*. 1996.
10. J. Stauber and T. Florence, *Marine Biology*, 1987, **94**, 511-519.
11. M. Löschau and R. Krätke, *Environmental Pollution*, 2005, **138**, 260-267.
12. L. Delauney, C. Compère and M. Lehaitre, *Ocean Science*, 2010, **6**, 503-511.
13. W. M. Dunne, *American Society for Microbiologist*, 2002, **15(2)**, 155-166
14. J. W. Costerton, G. G. Geesey, K. J. Cheng, *Scientific American*, 1978, **238(1)**, 86-95.
15. R. Coico, *Current Protocols in Microbiology*, 2005, **00(1)**.
16. S. Kumar. *Textbook of Microbiology*, JP Medical Ltd, London, 2012.
17. A. Umeda, Y. Ueki, K. Amako, *Journal of Bacteriology*, 1987, **169(6)**, 2482-2487
18. J. Raven and M. Giordano, *Current Biology*, 2014, **24**, 590-595.
19. O. P. Sharma, *Textbook of Algae*, Tata McGraw-Hill Education, New York, 1986.
20. S. Nishimoto and B. Bhushan, *RSC Adv.*, 2013, **3**, 671-690.
21. X. Zhang, L. Wang and E. Levänen, *RSC Advances*, 2013, **30**, 12003-12020.
22. W. Barthlott and C. Neinhuis, *Planta*, 1997, **202**, 1-8.
23. S. Bayoudh, A. Othmane, F. Bettaieb, A. Bakhrouf, H. Ouada and L. Ponsonnet, *Materials Science and Engineering: C*, 2006, **26**, 300-305.
24. A. Bavelloni, M. Piazzzi, M. Raffini, I. Faenza and W. Blalock, *IUBMB Life*, 2015, **67**, 239-254.
25. A. Tripathy, P. Sen, B. Su and W. Briscoe, *Advances in Colloid and Interface Science*, 2017, **248**, 85-104.
26. N. Aumsuwan, S. Heinhorst and M. Urban, *Biomacromolecules*, 2007, **8**, 3525-3530.
27. K. Poole, *Journal of Applied Microbiology*, 2002, **92**, 55-64.
28. P. Gong, H. Li, X. He, K. Wang, J. Hu, W. Tan, S. Zhang and X. Yang, *Nanotechnology*, 2007, **18**, 1-7.
29. A. Lansdown, *Journal of Wound Care*, 2002, **11**, 125-130.
30. M. Rai, A. Yadav and A. Gade, *Biotechnology Advances*, 2009, **27**, 76-83.
31. N. Durán, P. Marcato, G. De Souza, O. Alves and E. Esposito, *Journal of Biomedical Nanotechnology*, 2007, **3**, 203-208.
32. G. Watson, D. Green, L. Schwarzkopf, X. Li, B. Cribb, S. Myhra and J. Watson, *Acta Biomaterialia*, 2015, **21**, 109-122.

33. D. Green, K. Lee, J. Watson, H. Kim, K. Yoon, E. Kim, J. Lee, G. Watson and H. Jung, *Scientific Reports*, 2017, **7**.
34. E. Ivanova, J. Hasan, H. Webb, V. Truong, G. Watson, J. Watson, V. Baulin, S. Pogodin, J. Wang, M. Tobin, C. Löbbbe and R. Crawford, *Small*, 2012, **8**, 2489-2494.
35. J. Hasan, H. Webb, V. Truong, S. Pogodin, V. Baulin, G. Watson, J. Watson, R. Crawford and E. Ivanova, *Applied Microbiology and Biotechnology*, 2012, **97**, 9257-9262.
36. S. Kelleher, O. Habimana, J. Lawler, B. O' Reilly, S. Daniels, E. Casey and A. Cowley, *ACS Applied Materials & Interfaces*, 2015, **8**, 14966-14974.
37. E. Ivanova, J. Hasan, H. Webb, G. Gervinskas, S. Juodkasis, V. Truong, A. Wu, R. Lamb, V. Baulin, G. Watson, J. Watson, D. Mainwaring and R. Crawford, *Nature Communications*, 2013, **4**.
38. E. Ivanova, S. Nguyen, H. Webb, J. Hasan, V. Truong, R. Lamb, X. Duan, M. Tobin, P. Mahon and R. Crawford, *PLoS ONE*, 2013, **8**, e67893.
39. S. Pogodin, J. Hasan, V. Baulin, H. Webb, V. Truong, T. Phong Nguyen, V. Boshkovikj, C. Fluke, G. Watson, J. Watson, R. Crawford and E. Ivanova, *Biophysical Journal*, 2013, **104**, 835-840.
40. F. Xue, J. Liu, L. Guo, L. Zhang and Q. Li, *Journal of Theoretical Biology*, 2015, **385**, 01-7.
41. H. Jansen, M. Boer, R. Legtenberg and M. Elwenspoek, *Journal of Micromechanics and Microengineering*, 1995, **5**, 115-120.
42. J. Lv, T. Zhang, P. Zhang, Y. Zhao and S. Li, *Nanoscale Research Letters*, 2018, **13**.
43. C. Hsu, J. Wu, Y. Lu, D. Flood, A. Barron and L. Chen, *Materials Science in Semiconductor Processing*, 2014, **25**, 2-17.
44. R. Stephens and G. Cody, *Thin Solid Films*, 1977, **45**, 19-29.
45. J. Oh, H. Yuan and H. Branz, *Nature Nanotechnology*, 2012, **7**, 743-748.
46. P. May, M. Clegg, T. Silva, H. Zanin, O. Fatibello-Filho, V. Celorrio, D. Fermin, C. Welch, G. Hazell, L. Fisher, A. Nobbs and B. Su, *Journal of Materials Chemistry B*, 2016, **4**, 5737-5746.
47. Y. Yu, Z. Zhang, X. Yin, A. Kvit, Q. Liao, Z. Kang, X. Yan, Y. Zhang and X. Wang, *Nature Energy*, 2017, **2**.
48. E. Woerner, C. Wild, W. Mueller-Sebert and P. Koidl, *Diamond and Related Materials*, 2001, **10**, 557-560.
49. M. Zeren and Ş. Karagöz, *Materials & Design*, 2007, **28**, 1055-1058.
50. F. Bundy, *Science*, 1962, **137**, 1057-1058.
51. W. G. Eversole, US Pat. 3030187, 1958
52. J. Angus, H. Will and W. Stanko, *Journal of Applied Physics*, 1968, **39**, 2915-2922.
53. S. Matsumoto, Y. Sato, M. Tsutsumi and N. Setaka, *Journal of Materials Science*, 1982, **17**, 3106-3112.
54. J. Gracio, Q. Fan and J. Madaleno, *Journal of Physics D: Applied Physics*, 2010, **43**, 374017.
55. B. Waclawski, D. Pierce, N. Swanson and R. Celotta, *Journal of Vacuum Science and Technology*, 1982, **21**, 368-370.
56. P. May, *Philosophical Transactions of the Royal Society of London. Series A: Mathematical, Physical and Engineering Sciences*, 2000, **358**, 473-495.
57. I. Yagi, H. Notsu, T. Kondo, D. Tryk and A. Fujishima, *Journal of Electroanalytical Chemistry*, 1999, **473**, 173-178.
58. D. Zhu, J. Bandy, S. Li and R. Hamers, *Surface Science*, 2016, **650**, 295-301.
59. M. Salvadori, W. Araújo, F. Teixeira, M. Cattani, A. Pasquarelli, E. Oks and I. Brown, *Diamond and Related Materials*, 2010, **19**, 324-328.

60. 9.I. Iatsunskyi, S. Jurga, V. Smyntyna, M. Pavlenko, V. Myndrul and A. Zaleska, *Optical Micro- and Nanometrology V*, 2014, **9132**.
61. 10.J. Budil, P. Matyska Lišková, A. Artemenko, E. Ukrainsev, I. Gordeev, J. Beranová, I. Konopásek and A. Kromka, *Diamond and Related Materials*, 2018, **83**, 87-93.

#### Figures

1. R. Donlan, *Emerging Infectious Diseases*, 2002, **8**, 881-890.
2. BioNinja, <https://ib.bioninja.com.au/options/untitled/b1-microbiology-organisms/gram-staining.html>, (accessed 4/12/19)
3. Pixabay, <https://pixabay.com/photos/lotus-leaf-water-drop-lotus-water-2420205/> (accessed 8/4/20)